Quaternary Science Reviews
June 2022, Volume 286 Pages 107508 (15p.)
https://doi.org/10.1016/j.quascirev.2022.107508
https://archimer.ifremer.fr/doc/00772/88383/

Dust correlation and oxygen isotope stratigraphy in the Southern Ocean over the last 450 kyrs: An Indian sector perspective

Matsui Hiroki [1, 2, *], Ikehara Minoru [2], Suganuma Yusuke [3, 4], Seki Osamu [5], Oyabu Ikumi [3], Kawamura Kenji [3, 4]

[1] Graduate School of International Resource Sciences, Akita University, Tegatagakuen-machi 1-1, Akita 010-8502, Japan
[2] Center for Advanced Marine Core Research, Kochi University, B200 Monobe, Nankoku, Kochi 783-8502, Japan
[3] National Institute of Polar Research, Research Organizations of Information and Systems, Midori-cho 10-3, Tachikawa, Tokyo 190-8518, Japan
[4] Department of Polar Science, School of Multidisciplinary Sciences, The Graduate University for Advanced Studies (SOKENDAI), Midori-cho 10-3, Tachikawa, Tokyo, 190-8518, Japan
[5] Institute of Low Temperature Science, Hokkaido University, N19W8, Kita-ku, 8, Sapporo 060-0819, Japan

* Corresponding author : Hiroki Matsui, email address : hmatsui@gipc.akita-u.ac.jp

ikehara@kochi-u.ac.jp ; suganuma.yusuke@nipr.ac.jp ; seki@pop.lowtem.hokudai.ac.jp ; oyabu.ikumi@nipr.ac.jp ; kawamura@nipr.ac.jp

Abstract :

The chronology of Southern Ocean (SO) marine sediment cores forms the basis of understanding the SO paleoceanography, with significant implications for global climate. Because tuning of the oxygen isotope (δ18O) record of a marine sediment core to a δ18O stack (δ18O stratigraphy) is difficult in the SO because of a general paucity of calcareous foraminifera, tuning of the dust proxy signal of a marine sediment core to the dust record of an ice core (dust correlation) is a promising way to construct an age–depth model. However, the reliability of dust correlation has not been established, especially beyond the last ∼300 kyrs, and such work has been performed more in the Atlantic and Pacific sectors of the SO than in the Indian sector. Here we present a new dust correlation using the rock magnetic record, together with continuous δ18O stratigraphy, for a marine sediment core in the Indian sector of the SO over the last ∼410 kyrs. The δ18O stratigraphy is consistent with the dust correlation within their chronological uncertainties, supporting the reliability of the latter chronology for glacial–interglacial timescales. However, the dust correlation often produces older ages than the δ18O stratigraphy by up to 3 kyrs (410–126 ka and 84–50 ka). We additionally compiled, based on dust correlation, available dust proxy records in the circum-Antarctic SO for the last 450 kyrs to discuss variations in the dust proxy record within the Indian sector and between all three sectors. For the Indian sector, there is a marked difference in dust proxy signals for Marine Isotope Stage (MIS) 6 between two cores that have markedly different latitudinal positions relative to the oceanic fronts. Increased biogenic magnetite production by iron fertilization in the Subantarctic Zone during MIS 6 may partly explain the difference between the two cores. For the circum-Antarctic SO, moving correlation coefficients were computed between the marine sediment-core dust proxy signals and the dust flux of an Antarctic ice core. Strong correlation was recognized for intervals of high dust flux in the ice core, except for MIS 6. Although minor, the slightly lower correlation in the Indian sector than in the other sectors indicates a contribution from local dust source and volcanic materials and thus suggests the necessity for caution when performing dust correlation in the Indian sector of the SO.

Highlights

► Oxygen isotope stratigraphy confirms the utility of dust correlation. ► Iron fertilization may be a key factor controlling dust proxy signals. ► Large-scale climate forcings control dust proxy signals in the Southern Ocean.

Keywords : Southern ocean, Dust correlation, Oxygen isotope stratigraphy

1. Introduction

Past climate changes in the Southern Ocean (SO) are key to understanding the global climate system through heat transport, deep-water circulation, and CO_2 uptake (e.g., Sarmiento et al., 2004; Sigman et al., 2010). Accurate reconstruction of the SO paleoceanography essentially depends on the reliability of marine sediment-core chronologies, which often utilize radiocarbon (^{14}C) dating and oxygen isotope ($\delta^{18}O$) stratigraphy (e.g., Lisiecki and Raymo, 2005; Stern and Lisiecki, 2014). However, the general lack of biogenic carbonate (including carbonate shells of foraminifera) in the SO marine sediments has hindered application of these methods and thus necessitated alternative ways to construct a robust chronology. The alternative methods applicable to marine sediments include alignment of sea surface temperature (SST) data to the deuterium (δD) record of Antarctic ice cores (e.g., Govin et al., 2009; Elderfield et al., 2012; Hayes et al., 2014), alignment of dust proxies such as magnetic susceptibility (MS), iron (Fe) content, and lithogenic flux to the dust record of Antarctic ice cores (e.g., Pugh et al., 2009; Martínez-Garcia et al., 2011; Weber et al., 2012; Anderson et al., 2014; Lamy et al., 2014; Xiao et al., 2016), and synchronization of paleointensity or cosmogenic ^{10}Be to cosmogenic isotopic records from ice cores (e.g., Stoner et al., 2000; Channell et al., 2009; Suganuma et al., 2010; Horiuchi et al., 2016). All of these methods allow the transfer of ice-core ages (e.g., Kawamura et al., 2007; Veres et al., 2013; Bazin et al., 2013) to marine sediment cores and direct comparison of climatic records between marine sediment cores and ice cores within chronological uncertainties.

Alignment of dust proxies to the dust record of Antarctic ice cores (hereafter dust correlation) has been increasingly applied to constrain the chronology in the Scotia Sea (e.g., Weber et al., 2012, 2014; Xiao et al., 2016) and in the circum-Antarctic (e.g., Pugh et al., 2009; Lamy et al., 2014). Dust proxies (rock magnetic record, Fe content, and lithogenic flux) have diverse origins including aeolian dust, ice rafted debris, volcanic materials, and biogenic magnetite (e.g., Bareille et al., 1994; Yamazaki and Ikehara, 2012; Weber et al., 2012; Kim et al., 2018). Despite the diverse origins, dust correlation is based on the remarkable similarity between the variations in dust proxies of marine sediment cores and the changes in the dust flux of Antarctic ice cores (e.g., Petit et al., 1990; Pugh et al., 2009), the latter of which at the Last Glacial Maximum mostly originated from South America, mainly Patagonia (e.g., Basile et al., 1997; Delmonte et al., 2004; Ohgaito et al., 2018; Oyabu et al., 2020). The similarity between circum-Antarctic marine sediment cores and Antarctic ice cores is attributed to large-scale atmospheric circulation, to increased glaciogenic dust, and to wind-driven current transport (e.g., Pugh et al., 2009; Lamy et al., 2014; Ohgaito et al., 2018). Nevertheless, verification of dust correlation has been limited to the last ~300 kyrs by comparison with multiple proxies including ^{14}C dating and the abundance of radiolarian or diatom species (Pugh et al., 2009; Xiao et al., 2016), whereas the dust proxy records of marine sediment cores and the dust records of Antarctic ice cores extend back over the last ~4 Myrs (Martínez-Garcia et al., 2011) and the last ~800 kyrs (Lambert et al., 2012), respectively. Moreover, available dust proxy records in marine sediment cores are more centered on the Atlantic and Pacific sectors of the SO (e.g., Pugh et al., 2009; Anderson et al., 2014; Lamy et al., 2014) than the Indian sector (e.g., Bareille et al., 1994; Thöle et al., 2019).

In this study, we performed both $\delta^{18}O$ stratigraphy and dust correlation for a marine sediment core from the Indian sector of the SO to investigate the reliability of its dust correlation on glacial–interglacial timescales over the last ~410 kyrs. We compared our results with available marine-sediment-core dust proxy records from the Indian sector, and we addressed the potential role of Fe fertilization in dust proxy records by considering the possible changes in the positions of marine sediment cores relative to oceanic fronts during past glacial periods. We discuss that increased biogenic magnetite production by Fe fertilization affected dust proxy signals in the Subantarctic Zone but not in the Antarctic Zone. We also compiled published dust proxy records for the Pacific and Atlantic sectors of the SO, and we examined whether there were any differences in the proxy signals between the three sectors (Indian, Pacific, and Atlantic) by means of linear and moving correlation coefficients between the proxy signals of marine sediment cores and the dust flux of the EPICA Dome C (EDC) Antarctic ice core.

2. Materials and Methods

We investigated sediment samples from piston core DCR-1PC (46°01'S, 44°15'E, 2632 m water depth) from the Del Caño Rise in the Indian sector of the SO. The core was obtained during the KH-10-7 Cruise using the Research Vessel *Hakuho-maru* from the Japan Agency for Marine-Earth Science and Technology (JAMSTEC) (Fig. 1). The site is currently located north of the Subantarctic Front (SAF) and Polar Front (PF) (Orsi et al., 1995; Park et al., 2019). The recovered core length was ~10.2 m, and calcareous ooze is the major lithology throughout the core, with varying amounts of siliceous components reflecting glacial–interglacial variations. All samples were freeze-dried, then gently wet-sieved using a 63-μm screen and oven-dried (<40°C).

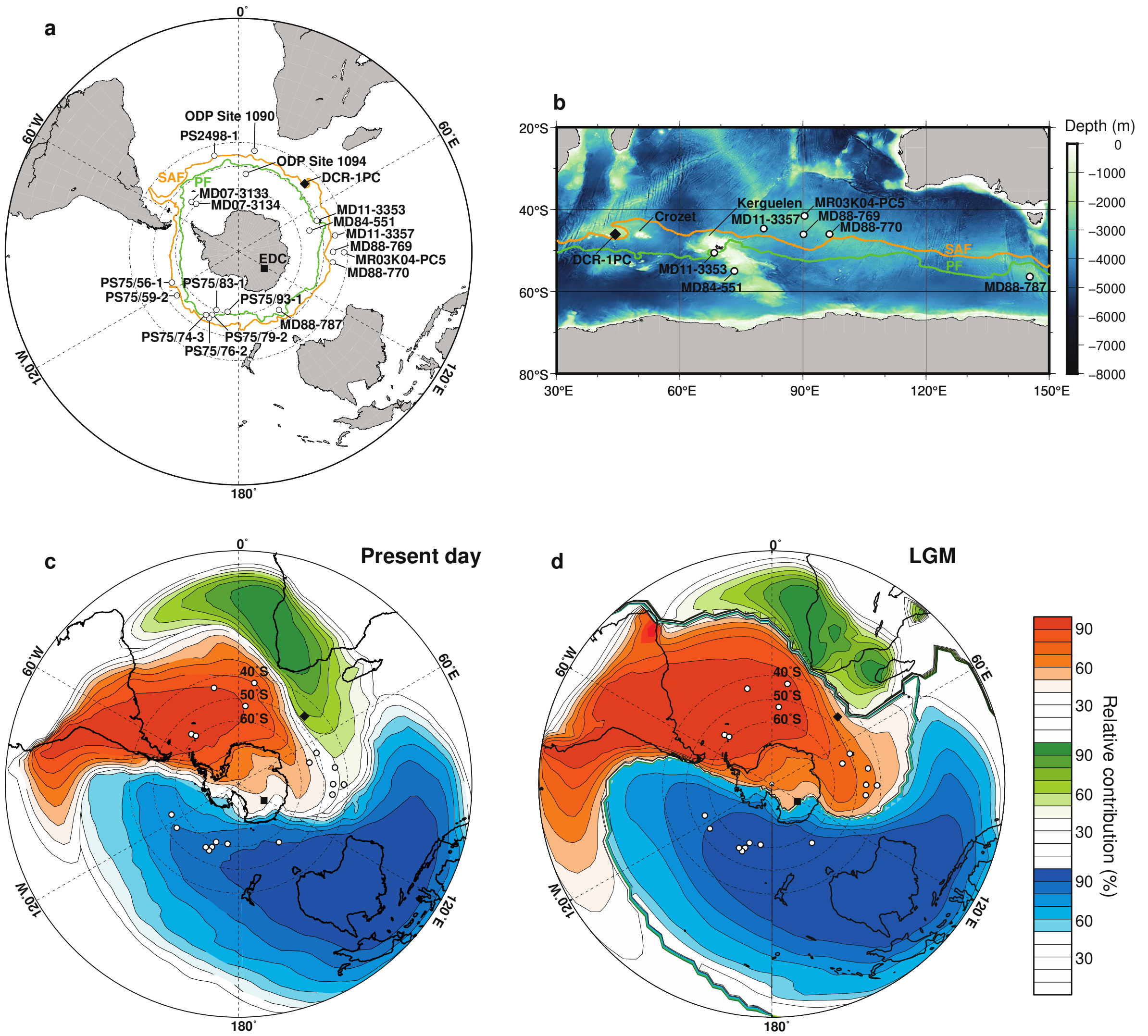

Fig. 1. (a) Core locations of the DCR-1PC core (black diamond) and compiled marine sediment cores (white circles) in the Southern Ocean (Table 1). The location of the EPICA Dome C (EDC) ice core is also shown (black square). Light orange and light green circles indicate the modern positions of the Subantarctic Front (SAF) and Polar Front (PF), respectively (Park et al., 2019). (b) Core locations and front positions in the Indian sector of the Southern Ocean. The Crozet and Kerguelen Plateaus are also shown. Bathymetry was plotted using GMT software (Wessel et al., 2013). (c) Relative contributions of the three Southern Hemisphere sources (red: South America; green: Africa; blue: Australia) to dust deposition at the present day (modified from Li et al., 2008). Core locations are the same as in (a). (d) Relative contributions of South America, Africa, and Australia to dust deposition at

the Last Glacial Maximum (LGM; modified from Li et al., 2010). Color shadings and core locations are the same as in (c).

Table 1. Southern Ocean marine sediment cores discussed in this study. Averages of sedimentation rate and sampling resolution are for 450 kyrs, based on dust correlation. Abbreviation: ARM, Anhysteretic remanent magnetization; MS, Magnetic susceptibility; MAR, Mass accumulation rate.

Number	Core	Sector	Latitude	Longitude	Water Depth (m)	Length (m)	Age range (kyr)	Ave. sed. rate (cm / kyr)
1	DCR-1PC	Indian	46˚01' S	44˚15' E	2632	10.2	413	2.5
2	MD11-3353	Indian	50˚34' S	68˚23' E	1568	11.3	133	8.5
3	MD84-551	Indian	55˚00' S	73˚20' E	2230	7.7	165	4.7
4	MD11-3357	Indian	44˚40' S	80˚25' E	3349	20.7	145	14.3
5	MD88-769	Indian	46˚04' S	90˚07' E	3420	16.5	201	8.2
6	MR03K04-PC5	Indian	41˚33' S	90˚24' E	2913	6.7	442	1.5
7	MD88-770	Indian	46˚01' S	96˚28' E	3290	16.8	231	7.3
8	MD88-787	Indian	56˚23' S	145˚18' E	3020	10.4	197	5.3
9	PS75/93-1	Pacific	60˚52' S	169˚32' W	3762	12.8	397	3.2
10	PS75/83-1	Pacific	60˚16' S	159˚03' W	3599	13.1	272	4.8

Ave. sampling resolution (kyr)	Dust proxy	References	Number	Core	Sector	Latitude	Longitude	Water Depth (m)	Length (m)	Age range (kyr)	Ave. sed. rate (cm / kyr)
0.92	ARM	Crosta et al., 2020; This study	11	PS75/79-2*	Pacific	57˚30' S	157˚14' W	3770	18.5	473	3.9
1.23	Fe	Thöle et al., 2019	12	PS75/76-2*	Pacific	55˚31' S	156˚08' W	3742	21.0	987	2.7
1.62	MS	Bareille et al., 1994	13	PS75/74-3*	Pacific	56˚14' S	152˚39' W	3295	21.0	1018	3.0
1.46	Fe	Thöle et al., 2019	14	PS75/59-2*	Pacific	54˚12' S	125˚25' W	3613	14.0	474	3.0
1.73	MS	Bareille et al., 1994	15	PS75/56-1	Pacific	55˚09' S	114˚47' W	3581	10.2	260	3.9
1.55	MS	Yamazaki and Ikehara, 2012	16	MD07-3133	Atlantic	57˚26' S	43˚27' W	3103	32.8	35	93.7
1.40	MS	Bareille et al., 1994	17	MD07-3134	Atlantic	59˚24' S	41˚28' W	3663	58.1	92	63.1
1.71	MS	Bareille et al., 1994	18	PS2498-1	Atlantic	44˚09' S	14˚13' W	3783	9.3	91	10.3
0.32	Fe	Lamy et al., 2014	19	ODP Site 1094*	Atlantic	53˚10' S	5˚07' E	2807.3	168.7	1558	16.2
0.22	Fe	Lamy et al., 2014	20	ODP Site 1090**	Atlantic	42˚54' S	8˚53' E	3700	25.5	800	3.1

Ave. sampling resolution (kyr)	Dust proxy	References
0.18	Fe	Lamy et al., 2014
0.26	Fe	Lamy et al., 2014
0.33	Fe	Lamy et al., 2014
0.20	Fe	Lamy et al., 2014; Ullermann et al., 2016
0.13	Fe	Lamy et al., 2014; Ullermann et al., 2016
0.01	MS	Weber et al., 2012
0.02	MS	Weber et al., 2012
0.34	Lithic flux	Gersonde et al., 2003; Anderson et al., 2014
1.41	Fe	Latimer et al., 2006; Hasenfratz et al., 2019
0.33	Fe MAR	Martínez-Garcia et al., 2011

*We compiled only the last 450 kyrs for comparison with the other sites.

**The age model beyond 800 ka is $\delta^{18}O$ stratigraphy. We compiled only the last 450 kyrs for comparison with the other sites.

2.1. Stable oxygen isotope measurements

The stable oxygen isotopic ratios of the benthic foraminifera *Cibicidoides wuellerstorfi* (0.01–0.36 m and 1.66 m depth) and *Melonis barleeanus* (0.01–10.16 m depth) were measured to construct an age–depth model for the DCR-1PC core (Section 4.1.). Because *C. wuellerstorfi*, which is an epifaunal species, was rare below 0.36 m, we chose the infaunal *M. barleeanus* to generate a continuous record (180–355 μm size fraction, 3–5 specimens). The average sampling resolution for *M. barleeanus* was 1.9 cm. Correction factors of +0.64‰ and +0.40‰ were applied to the $\delta^{18}O$ measurements of *C. wuellerstorfi* and *M. barleeanus*, respectively (Duplessy et al., 1984; Labeyrie et al., 1996).

A total of 554 samples (16 for *C. wuellerstorfi* and 538 for *M. barleeanus*) were cleaned with methanol by ultrasonication, gently crushed, and then mixed to homogenize the foraminiferal tests before isotopic analysis. All stable isotope measurements were performed using an online system employing an IsoPrime isotope-ratio mass spectrometer (GV

Instruments Ltd.) coupled to a Multicarb automatic sample treatment system (Center for Advanced Marine Core Research [CMCR], Kochi University, Japan). The isotopic values are reported in δ notation relative to the Vienna Pee Dee Belemnite international standard. The analytical precision of the measurements was ±0.10‰.

2.2. Rock magnetic measurements and non-destructive measurements

Anhysteretic remanent magnetization (ARM) and isothermal remanent magnetization (IRM) were measured on 448 discrete cube samples at the National Institute of Polar Research, Japan, to estimate the magnetic grain concentrations for dust correlation (Section 4.2.). ARM acquisition was performed in a 0.03-mT DC field with an 80-mT AF using an SRM-760R magnetometer. The IRM was imparted at 1.5 T using a pulse magnetizer (MMPM-9; Magnetic Measurements, UK) and measured by a spinner magnetometer (Natsuhara-Giken SMD-88). The average sampling resolution for the measurements was 2.2 cm, which is comparable with the resolution of the $\delta^{18}O$ record. The ARM record is thought to reflect the concentration of ferrimagnetic material, especially smaller magnetite grains (<10 μm) (Stoner and St-Onge, 2007), which are the main carriers of magnetization and are the likely source of MS (Mazaud et al., 2002; Pugh et al., 2009). We also conducted non-destructive measurements of Fe_2O_3 and MS at CMCR, Kochi University, to allow comparison of dust proxies. Fe_2O_3 and MS were measured at 1-cm intervals using an X-ray fluorescence scanner JEOL TATSCAN-F2 (Sakamoto et al., 2006) and a multi-sensor core logger (MSCL-S, GEOTEK Ltd.; sensor, Bartington Instruments Ltd.), respectively.

2.3. Compilation of dust proxy records in the Southern Ocean

We compiled a total of 19 dust proxy records for marine sediment cores in the SO (south of 40°S, >1500 m water depth) (Fig. 1; Table 1) to consider possible sector-scale differences.

Seven sites were located in the Indian sector (68°E to 145°E, 41°S to 56°S) (Bareille et al., 1994; Yamazaki and Ikehara, 2012; Thöle et al., 2019), seven in the Pacific sector (169°W to 114°W, 54°S to 60°S) (Lamy et al., 2014; Ullermann et al., 2016), and five in the Atlantic sector (43°W to 8°E, 42°S to 59°S) (Latimer et al., 2006; Martínez-Garcia et al., 2011; Weber et al., 2012; Anderson et al., 2014; Hasenfratz et al., 2019). Compiled records are limited to the last 450 kyrs, and each age model is based on dust correlation, $\delta^{18}O$ stratigraphy, or δD–SST correlation (Table 2). For the PS2498-1 core, the age model also includes ^{14}C dates (Gersonde et al., 2003; Anderson et al., 2014). Linear correlation coefficients between the marine sediment-core dust proxy signals and the EDC ice core dust flux (Lambert et al., 2012) were computed after each record had been resampled every 1 kyr (Table 2).

Table 2. Correlation coefficients for the last 450 kyrs between dust proxy signals (linear scale) based on each age model and the EDC dust flux (log scale). Dust correlation using the Match program (Lisiecki and Lisiecki, 2002) are in bold (see Section 4.2). Correlation coefficients for the last 100 kyrs based on dust correlation were also calculated (see Section 5.3).

Number	Core	Age model	Correlation (*r*) for 450 kyrs	Correlation (r) for 100 kyrs
1	DCR-1PC	^{14}C, δD–SST correlation	0.50	
		^{14}C, $\delta^{18}O$ stratigraphy	0.59	
		Dust correlation	0.64	0.72
2	MD11-3353	δD–SST correlation	0.68	
		Dust correlation	0.74	0.75
3	MD84-551	$\delta^{18}O$ stratigraphy	0.63	
		Dust correlation	0.70	0.55
4	MD11-3357	δD–SST correlation	0.72	
		Dust correlation	0.81	0.77
5	MD88-769	$\delta^{18}O$ stratigraphy	0.48	
		Dust correlation	0.69	0.66

6	MR03K04-PC5	$\delta^{18}O$ stratigraphy	0.52	
		Dust correlation	0.67	0.73
7	MD88-770	$\delta^{18}O$ stratigraphy	0.40	
		Dust correlation	0.53	0.56
8	MD88-787	$\delta^{18}O$ stratigraphy	0.51	
		Dust correlation	0.51	0.63
9	PS75/93-1	Dust correlation	0.70	0.73
10	PS75/83-1	Dust correlation	0.72	0.74
11	PS75/79-2	Dust correlation	0.77	0.74
12	PS75/76-2	Dust correlation	0.78	0.84
13	PS75/74-3	Dust correlation	0.73	0.58
14	PS75/59-2	$\delta^{18}O$ stratigraphy	0.58	
		Dust correlation	0.62	0.74
15	PS75/56-1	$\delta^{18}O$ stratigraphy	0.54	
		Dust correlation	0.68	0.68
16	MD07-3133	Dust correlation	0.90	0.90
17	MD07-3134	Dust correlation	0.71	0.71
18	PS2498-1	^{14}C, Dust correlation	0.81	0.81
19	ODP Site 1094	$\delta^{18}O$ stratigraphy	0.65	
		Dust correlation	0.70	0.75
20	ODP Site 1090	Dust correlation	0.75	0.84

3. Results

3.1. Stable oxygen isotope ratios of benthic foraminifera

Oxygen isotope measurements for the benthic foraminifera *C. wuellerstorfi* were limited to the upper part of the DCR-1PC core, whereas *M. barleeanus* recorded $\delta^{18}O$ variations throughout the core (except for 5.23–5.57 m depth) (Fig. 2; Table S1). For the interval from 0.01 to 0.36 m depth, both *C. wuellerstorfi* and *M. barleeanus* show similar $\delta^{18}O$ values, supporting use of the latter species for correlation with the benthic $\delta^{18}O$ stack (hereafter LR04) (Lisiecki and Raymo, 2005). The corrected $\delta^{18}O$ values (+0.40‰) of *M. barleeanus* ranged from 2.84‰ (at 3.22 m depth) to 5.17‰ (at 0.45 m depth), whereas the LR04 varied from 3.10‰ (at 123 ka) to 5.02‰ (at 18 ka) through the last 800 kyrs (Lisiecki and Raymo, 2005; Past Interglacials Working Group of PAGES, 2016).

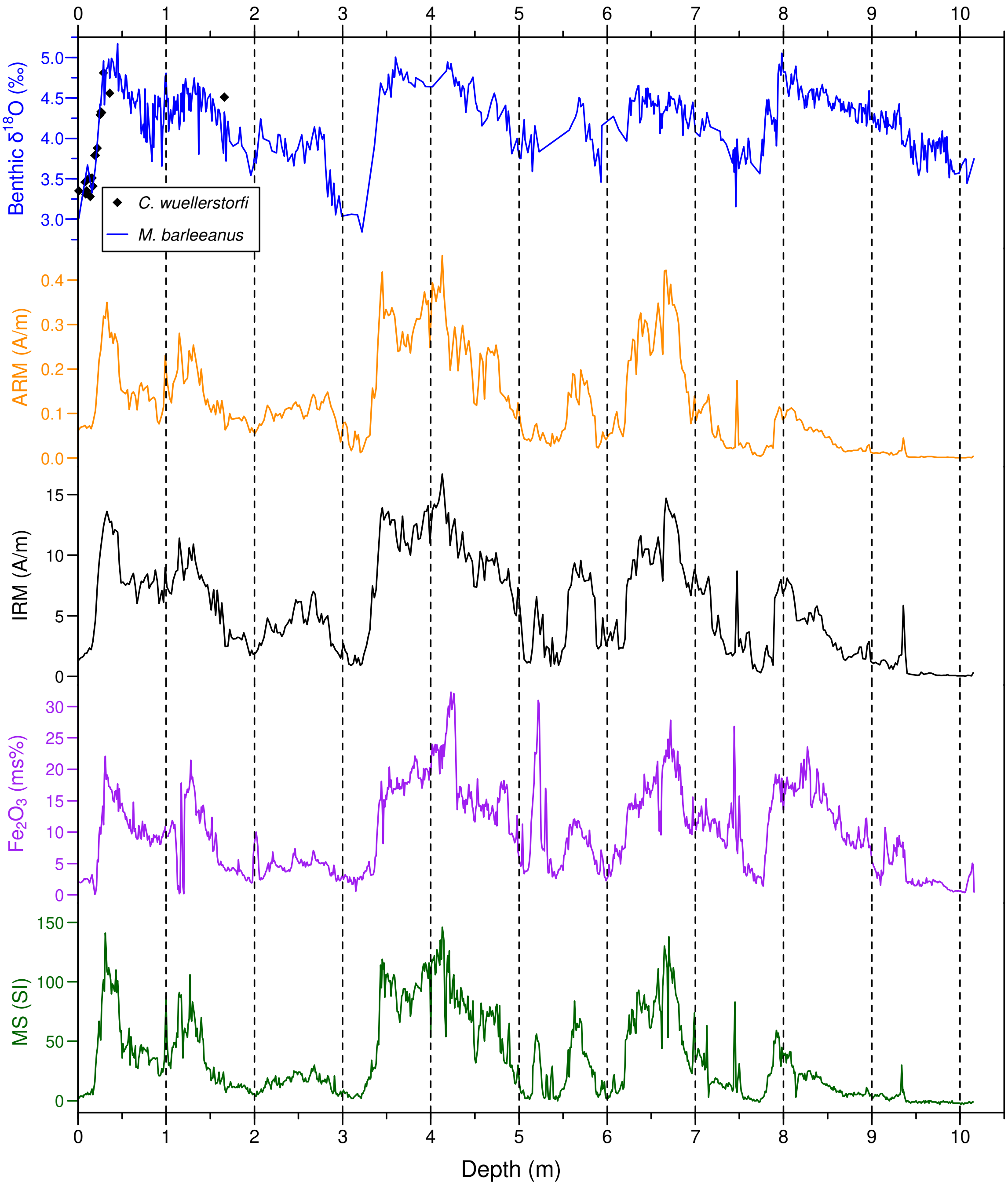

Fig. 2. Stable oxygen isotope ratio ($\delta^{18}O$) measurements of benthic foraminifera, rock magnetic measurements (ARM and IRM), and non-destructive measurements (Fe_2O_3 and MS) for the DCR-1PC core. Correction factors of +0.64‰ and +0.40‰ were applied to the $\delta^{18}O$ measurements of *C. wuellerstorfi* and *M. barleeanus*, respectively (Duplessy et al.,

1984; Labeyrie et al., 1996).

3.2. Variations in the dust proxy records (ARM, IRM, Fe_2O_3, and MS)

All the dust proxy records in the DCR-1PC core exhibited marked fluctuations, reflecting glacial–interglacial variations (Fig. 2; Table S2). The ARM ranged from 4.75×10^{-4} to 4.55×10^{-1} A/m (average 1.23×10^{-1} A/m) and the IRM from 0.04 to 16.7 A/m (average 5.7 A/m). Fe_2O_3 varied from 0.09 to 32.3 ms% (average 10.0 ms%) and MS from -3 to 146 SI (average 35 SI). Although the amplitudes of the peaks differ slightly among the records (e.g., the amplitude of the peaks at ~8 m between ARM and Fe_2O_3), any two of the records are well correlated ($0.67 < r < 0.95$) and each record markedly resembles the dust flux of the EDC Antarctic ice core (Lambert et al., 2012).

4. Age–depth models

4.1. $\delta^{18}O$ stratigraphy

We constructed an age–depth model for the DCR-1PC core by using a combination of available ^{14}C dates (Crosta et al., 2020) for the last 50 kyrs and graphic correlation of the $\delta^{18}O$ measurements of *M. barleeanus* to the LR04 (Lisiecki and Raymo, 2005) for the older ages using some of the maxima and minima as well as the absolute values (Fig. 3a). The number of $\delta^{18}O$ tie points (n = 9) was minimal to avoid abrupt changes in the linear sedimentation rates (LSRs). Comparison between our $\delta^{18}O$ profile for the constructed age model (hereafter $\delta^{18}O$ age model) and the LR04 suggests continuous sediment deposition at the studied site covering the last ~410 kyrs (Fig. 3a; Table 3). The correlation coefficient (r) between the $\delta^{18}O$ of *M. barleeanus* (resampled every 1 kyr) and the LR04 is 0.85. The LSRs ranged from 0.82 to 3.41 cm/kyr (average 2.48 cm/kyr) (Fig. 3c; Table 3). Compared to the LR04, the $\delta^{18}O$ values of *M. barleeanus* were heavier by ~0.5‰ during Marine Isotope

Stages (MIS) 11 (410–396 ka) and by ~0.4‰ during MIS 9 (337–321 ka), and lighter by ~0.3‰ during MIS 5 (129–112 ka). During MIS 3 (57–29 ka), the $\delta^{18}O$ of *M. barleeanus* displayed higher variability than during the other MISs (MIS 11–1).

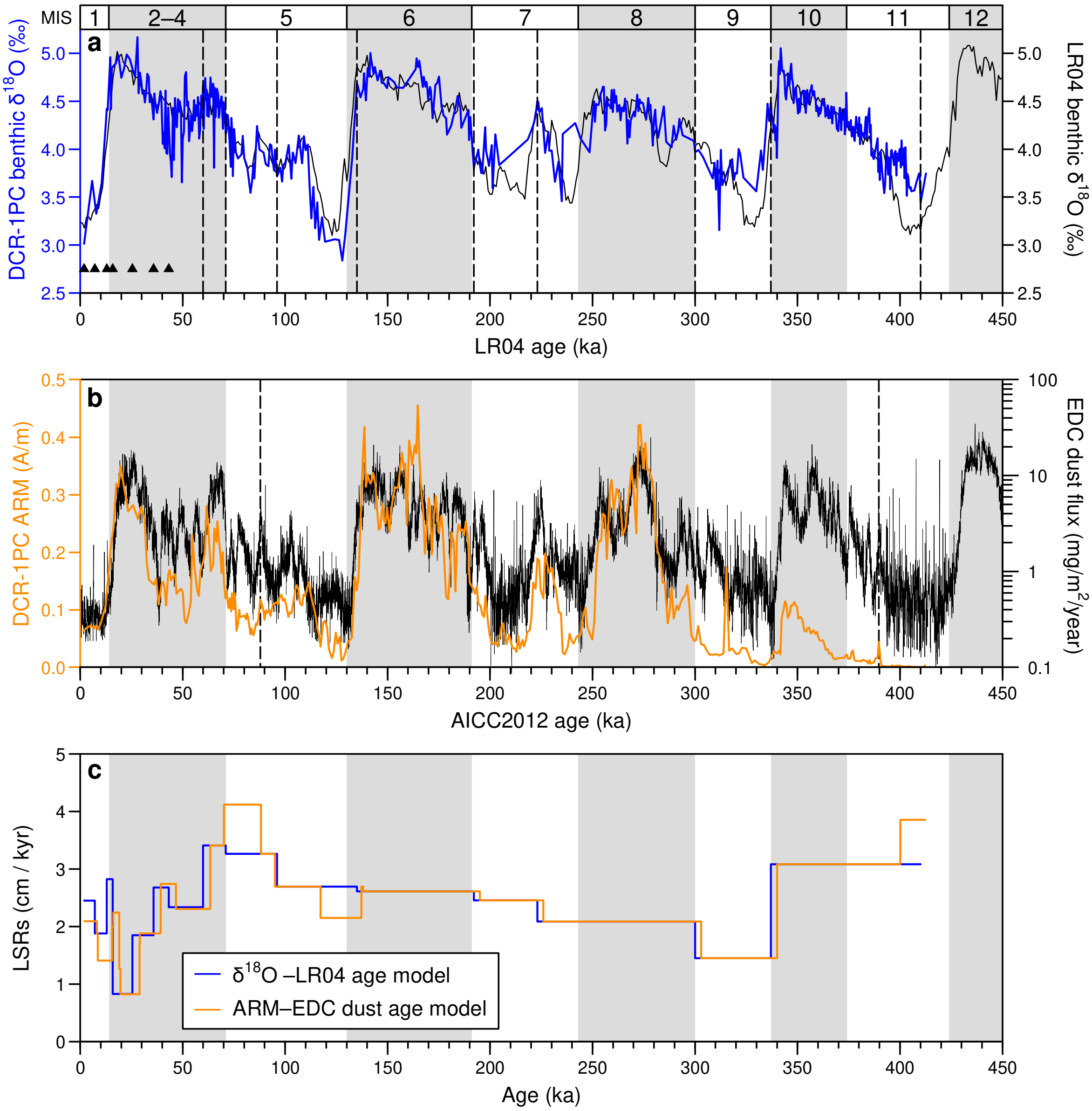

Fig. 3. (a) Graphic correlation (nine tie points, vertical dashed lines) between DCR-1PC benthic $\delta^{18}O$ (blue line) and the LR04 (black line) (Lisiecki and Raymo, 2005). Seven triangles indicate radiocarbon ages of planktic foraminifera from the DCR-1PC core (Crosta et al., 2020). (b) Signal matching (two tie points, vertical dashed lines) between the ARM of the DCR-1PC core (orange line) and the EDC dust flux (black line) (Lambert et al., 2012) on

the AICC2012 timescale (Veres et al., 2013; Bazin et al., 2013). (c) Linear sedimentation rates (LSRs) based on the two age–depth models. The boundary ages of each Marine Isotope Stage (MIS) follow Lisiecki and Raymo (2005), and glacial intervals are indicated by gray bars.

Table 3. Radiocarbon dating (Crosta et al., 2020) and tie points of $\delta^{18}O$ stratigraphy in the DCR-1PC core. Linear sedimentation rates (LSRs) are also provided.

Depth (m)	Age (ka)	LSR (cm / kyr)	Methods	References
0.01	1.864	2.61	Radiocarbon	Crosta et al., 2020
0.14	7.173	1.76	Radiocarbon	Crosta et al., 2020
0.25	13.019	2.81	Radiocarbon	Crosta et al., 2020
0.33	15.853	0.82	Radiocarbon	Crosta et al., 2020
0.41	25.517	1.88	Radiocarbon	Crosta et al., 2020
0.60	35.795	2.74	Radiocarbon	Crosta et al., 2020
0.80	43.258	2.31	Radiocarbon	Crosta et al., 2020
1.19	60.0	3.41	$\delta^{18}O$ stratigraphy	This study
1.57	71.0	3.27	$\delta^{18}O$ stratigraphy	This study
2.38	96.0	2.69	$\delta^{18}O$ stratigraphy	This study
3.43	135.0	2.61	$\delta^{18}O$ stratigraphy	This study
4.92	192.0	2.46	$\delta^{18}O$ stratigraphy	This study
5.68	223.0	2.09	$\delta^{18}O$ stratigraphy	This study
7.29	300.0	1.45	$\delta^{18}O$ stratigraphy	This study
7.83	337.0	3.08	$\delta^{18}O$ stratigraphy	This study
10.08	410.0		$\delta^{18}O$ stratigraphy	This study

4.2. Dust correlation

The ARM record of the DCR-1PC core on the $\delta^{18}O$ age model (Section 4.1.) was aligned to the EDC dust flux record (Lambert et al., 2012) on the AICC2012 timescale (Veres et al., 2013; Bazin et al., 2013) (Fig. 3b) using the Match program (Lisiecki and Lisiecki, 2002). The Match utilizes dynamic programming to find the optimal alignment between the signal (i.e., the ARM) and the target (i.e., the EDC dust flux). We first normalized the ARM on a linear scale and the EDC dust flux on a log scale (to capture the small fluctuations during interglacial periods) to have zero mean and one standard deviation, and then matched the ARM to the EDC dust flux with penalty functions to constrain LSRs (Fig. 3b; Table S3). We also added two tie points based on the peaks between the ARM and the EDC dust flux (Fig. 3b and Table S3). The resulting age–depth model (hereafter dust age model) (Table 4) compares well with the $\delta^{18}O$ stratigraphy (Fig. 4). The correlation coefficient between the ARM and the EDC dust flux (both records resampled every 1 kyr) is $r = 0.64$ on the dust age model, which is larger than that before the matching ($r = 0.59$) (Table 2). The LSRs ranged from 0.82 to 4.12 cm/kyr (average 2.35 cm/kyr) (Fig. 3c). Compared to the EDC dust flux (Lambert et al., 2012), the ARM values are relatively lower for MIS 10, given the higher ARM values for the other glacial periods (MIS 8, 6, and 2–4) (Fig. 3b). Reductive dissolution of magnetic minerals below the Fe-redox boundary (e.g., Yamazaki et al., 2003) may have occurred for this interval (i.e., MIS 10).

We also constructed dust age models for seven sites (MR03K04-PC5 and the six MD cores) in the Indian sector and for Ocean Drilling Program (ODP) Site 1094 in the Atlantic sector by matching the dust proxy signals (i.e., MS and Fe) (Bareille et al., 1994; Latimer et al., 2006; Yamazaki and Ikehara, 2012; Thöle et al., 2019) to the EDC dust flux (Lambert et al., 2012) in the same manner as for the DCR-1PC core, without adding any tie points. The linear correlation coefficients between the eight dust proxy signals and the EDC dust flux were mostly increased after matching, as expected (Table 2).

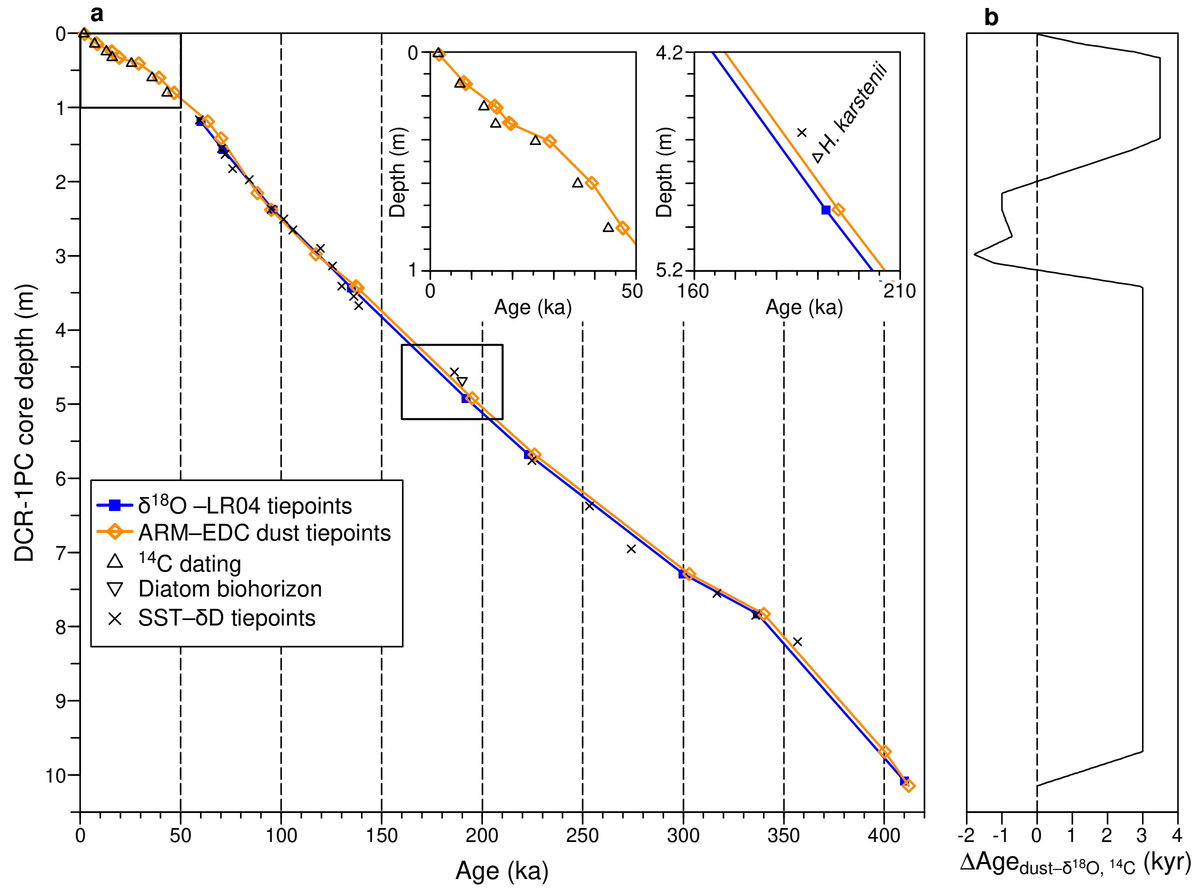

Fig. 4. Age–depth model comparison for the DCR-1PC core. (a) Benthic $\delta^{18}O$ age model (blue squares and lines) and dust age model (orange diamonds and lines). The uncertainties of the LR04 timescale (Lisiecki and Raymo, 2005) and the AICC2012 timescale (Veres et al., 2013; Bazin et al., 2013) are shown in light blue and light orange, respectively. Radiocarbon (^{14}C) dating of planktic foraminifera, the tie points of δD–SST correlation, and the last abundant appearance datum of the diatom *Hemidiscus karstenii* are also shown (Crosta et al., 2020). The insets show expanded views for 210–160 ka and 50–0 ka. (b) Age differences (ΔAge) between the dust age model and the $\delta^{18}O$ age model for 410–50 ka and between the dust age model and the ^{14}C ages for 50–0 ka. Positive values indicate that the dust age model is older than the $\delta^{18}O$ age model (or ^{14}C age) at the same depth; negative values indicate that the dust age model is younger.

Table 4. Tie points of dust correlation for the DCR-1PC core. Linear sedimentation rates (LSRs) are also provided.

Depth (m)	Age (ka)	LSR (cm / kyr)
0.01	2.1	0.57
0.14	8.1	1.70
0.15	8.6	1.71
0.25	15.6	1.57
0.26	16.1	1.59
0.32	19.1	1.69
0.33	19.6	1.68
0.41	29.0	1.40
0.41	29.1	1.40
0.60	39.2	1.53
0.60	39.3	1.53
0.80	46.7	1.72
0.81	46.8	1.72
1.19	63.5	1.88
1.42	70.1	2.02
2.16	88.1	2.45
2.38	95.0	2.51
2.98	117.2	2.54
3.41	137.2	2.49
3.43	138.0	2.49
4.92	195.0	2.52
5.68	226.0	2.51
7.29	303.0	2.41
7.83	340.0	2.30
9.68	400.2	2.42
10.15	412.2	

5. Discussion

5.1. Comparison of age–depth models of the DCR-1PC core

The DCR-1PC core (46°01'S, 44°15'E) yielded a sufficient amount of carbonate and siliceous microfossils (Crosta et al., 2020; Itaki et al., 2020; Shukla et al., 2021; this study) and preserved obvious dust proxy signals (Fig. 2), making it suitable for comparison of various age–depth models. A previous study on the core presented seven ^{14}C dates for 50–0 ka and twenty tie points from the alignment of the diatom-based summer SST record to the δD record of the EDC (Jouzel et al., 2007) for 360–50 ka (Crosta et al., 2020). We constructed the $\delta^{18}O$ age model and dust age model over the last ~410 kyrs.

5.1.1. Comparison of the $\delta^{18}O$ age model with the ^{14}C and δD–SST age models

First, we checked the ^{14}C ages for the last 50 kyrs (Crosta et al., 2020) by comparing with the published $\delta^{18}O$ stacks. The ^{14}C-dated benthic $\delta^{18}O$ in the DCR-1PC core closely follows the LR04 in both the timing of deglacial transition and the absolute values (Fig. 3a). The benthic $\delta^{18}O$ in the DCR-1PC core (2632 m water depth) is also consistent with the Deep (>2000 m water depth) Indian benthic $\delta^{18}O$ stack of Stern and Lisiecki (2014) (Fig. S1), although the marine reservoir ages adopted were 890 years for the DCR-1PC core (Crosta et al., 2020) and 405 years in the Deep Indian $\delta^{18}O$ stack (Stern and Lisiecki, 2014). The consistency with the published $\delta^{18}O$ stacks supports the robustness of ^{14}C dating for the DCR-1PC core.

Next, we considered the relationship between the $\delta^{18}O$ age model (this study) and the δD–SST alignment (Crosta et al., 2020) for 360–50 ka (Fig. 4a). The $\delta^{18}O$ age model is generally in good agreement with the tie point ages from the δD–SST alignment considering the underlying uncertainties of the LR04 timescale (4.0 kyrs as one sigma; Lisiecki and Raymo, 2005) and the AICC2012 timescale (0.8–3.9 kyrs as one sigma; Veres et al., 2013; Bazin et al., 2013). A notable difference is present for the last abundant appearance datum of the diatom *Hemidiscus karstenii*, which is dated to ~183 ka based on the $\delta^{18}O$ age model (this study) but to ~190 ka based on the δD–SST alignment (Crosta et al., 2020) (Fig. 4a inset).

However, the difference does not conflict with the published age range of 190–180 ka for the datum in the Atlantic Sector of the SO (Zielinski and Gersonde, 2002). Thus, we confirm the utility of the δD–SST age model for glacial–interglacial timescales (Thöle et al., 2019), apart from the age model uncertainties, which include possible diachronous surface water and surface air temperature changes (Govin et al., 2015).

5.1.2. Comparison of the dust age model with the ^{14}C, δD–SST, and $\delta^{18}O$ age models

First, we compared the dust age model with the ^{14}C ages for 50–0 ka (Fig. 4a inset). The dust age model for before 7 ka is older than the ^{14}C ages by up to 3.5 kyrs (Fig. 4b). The age differences exceed the uncertainties of the underlying AICC2012 chronology (0.2 to 1.1 kyrs, one sigma) (Veres et al., 2013) for the dust age model and of the ^{14}C dating (up to 0.3 kyrs, one sigma) (Crosta et al., 2020). Therefore, either overestimation of the dust age model or underestimation of the ^{14}C ages is the likely reason for the discrepancy between the two chronologies.

Taking into consideration that the ^{14}C ages are consistent with the published $\delta^{18}O$ stacks (Section 5.1.1.), overestimation of the dust age model may appear to be more likely. However, ^{14}C dating of foraminifera may yield markedly (a few kiloyears) younger ages if bioturbation such as *Zoophycos* occurs near the seafloor (e.g., Lowemark and Grootes, 2004; Lougheed et al., 2018), which may be important, especially at low-sedimentation-rate sites such as DCR-1PC (~2.5 cm/kyr). Thus, it is difficult to determine whether the discrepancy between the two chronologies arises from the error in the dust age model (potential overestimation) or from ^{14}C dating (potential underestimation) without further research on bioturbation processes at the DCR-1PC core and/or age–depth model comparisons of cores with higher sedimentation rates (>10 cm/kyr).

Beyond the ^{14}C dating (i.e., older than ~50 ka), the dust age model is generally consistent with the tie point ages of the δD–SST alignment (Crosta et al., 2020) as for the comparison between the $\delta^{18}O$ age model and the δD–SST alignment (Fig. 4a). The diatom *H. karstenii* datum is estimated as ~186 ka based on the dust age model (this study), which falls between the values of ~183 ka from the $\delta^{18}O$ age model and ~190 ka from the δD–SST alignment (Fig. 4a inset).

Finally, we assessed the differences between the dust and $\delta^{18}O$ age models for 410–50 ka (Fig. 4b). The dust age model shows older ages than the $\delta^{18}O$ age model by up to 3 kyrs. A clear exception is seen for the 2.00–3.18 m depth interval (84.3–125.6 ka on the $\delta^{18}O$ age model), where the dust age model yields a younger age than the $\delta^{18}O$ age model by up to 1.8 kyrs. Assuming the underlying uncertainties of the AICC2012 timescale (0.8–4.8 kyrs as one sigma; Veres et al., 2013; Bazin et al., 2013) and the LR04 timescale (4.0 kyrs as one sigma; Lisiecki and Raymo, 2005), the two age–depth models for the DCR-1PC core are consistent with each other within the uncertainties (i.e., ~4.1–6.2 kyrs). Therefore, dust correlation can be applied to the DCR-1PC site in the Indian sector of the SO for glacial–interglacial timescales at least over the last ~410 kyrs.

5.2. Dust proxy signals in the Indian sector of the SO

Dust correlation has been most commonly applied in the Atlantic sector of the SO because of the area's proximity to the South American (mainly Patagonian) dust source (e.g., Pugh et al., 2009; Martínez-Garcia et al., 2011; Weber et al., 2012; Anderson et al., 2014) which dominantly contributed to the EDC dust flux during the past glacial periods (e.g., Delmonte et al., 2004, 2008). Attempts to reconstruct dust proxy signals from the Pacific sector of the SO have also been made, for which the likely dust sources are Australia and New Zealand (e.g., Pugh et al., 2009; Lamy et al., 2014). The longest dust proxy records cover ~4 Myrs in the Atlantic sector (Martínez-Garcia et al., 2011) and ~1 Myr in the Pacific sector (Lamy et al., 2014).

For the Indian sector of the SO, however, potential sources of dust proxy signals are more complex, and may include dust from South America and South Africa and volcanic materials from the Crozet and Kerguelen Plateaus (e.g., Bareille et al., 1994; Thöle et al., 2019) (Fig. 1). In addition, most of the dust proxy records cover only the last ~200 kyrs (e.g., Petit et al., 1990; Bareille et al., 1994; Pugh et al., 2009), except for the MR03K04-PC5 core that covers the last ~440 kyrs (Yamazaki and Ikehara, 2012). We compiled published dust proxy records (n = 7) for comparison with the DCR-1PC core, which provides the dust proxy record over the last ~410 kyrs. The average sampling resolution is highest for the DCR-1PC site (0.92 kyr), compared to 1.23–1.73 kyr for the compiled seven sites (Table 1).

The dust proxy records from the eight sites in the Indian sector show site-specific variations with overall similarity ($0.51 < r < 0.81$) with the EDC dust flux variations (Lambert et al., 2012) (Figs. 1b, 5). The general similarities can be explained by the extended Patagonian dust source during past glacial periods (Li et al., 2008, 2010; Ohgaito et al., 2018) (Fig. 1d), except for the MD 88-787 core, which would have been more influenced by Australian and New Zealand dust sources. We should note, however, that the dust proxy signals of the Indian sector can also be controlled by volcanic materials from the Crozet and Kerguelen Plateaus (Fig. 1b). For the DCR-1PC core, which is located west of the plateaus, the contribution of volcanic materials from the plateaus is expected to be small because the materials are transported mainly eastward by the Antarctic Circumpolar Current (Bareille et al., 1994; Dezileau et al., 2000). For the MR03K04-PC5 core, biogenic magnetite dominates the magnetic mineral assemblage, suggesting a limited contribution of volcanic material (Yamazaki and Ikehara, 2012). Thus, any difference in the dust proxy records between the DCR-1PC and MR03K04-PC5 cores is likely not caused by material inputs from the Crozet and Kerguelen Plateaus.

There is a marked difference between the dust proxy records of the DCR-1PC and MR03K04-PC5 cores for MIS 6 (Fig. 5). The MR03K04-PC5 core has a broader peak centered in the first half of MIS 6 (~190–160 ka), whereas the DCR-1PC core has a peak centered in the latter half of MIS 6 (~170–135 ka); the latter peak is consistent with the EDC dust flux (Lambert et al., 2012). Although less visible, peaks in the MR03K04-PC5 core also precede peaks in the DCR-1PC core during MIS 2, 8, and 10 (Fig. 5). We here consider the positions of these cores relative to the oceanic fronts (SAF and PF) as a potential reason for their different dust proxy records. The DCR-1PC site is located ~1° and ~4° north of the modern SAF and PF, respectively, whereas the MR03K04-PC5 site is located ~8° and ~11° north of the modern SAF and PF, respectively (Park et al., 2019) (Fig. 1). If northward migration of the SAF and PF by 4–5° also occurred during MIS 6, as reconstructed for the Last Glacial Maximum (e.g., Gersonde et al., 2003, 2005; Kohfeld et al., 2013; Civel-Mazens et al., 2021), the DCR-1PC site would have been south of the SAF and at or south of the PF (i.e., the Antarctic Zone), and the MR03K04-PC5 site would still have been located north of the SAF and PF (i.e., in the Subantarctic Zone). This interpretation of the relative positions of the two sites with respect to the fronts can be tested by means of the lithologies of the two cores, because calcareous ooze dominates north of the PF and diatom ooze south of the PF (e.g., Burckle and Cirilli, 1987; Diekmann, 2007). The alteration of calcareous nannofossil ooze and diatom ooze in the DCR-1PC core (Crosta et al., 2020; this study) and the dominance of foraminifera-bearing calcareous nannofossil ooze in the MR03K04-PC5 core (Yamazaki and Ikehara, 2012) suggest that the former site was located in the Antarctic Zone and the latter site in the Subantarctic Zone during MIS 6 and other glacial periods.

During past glacial periods, the aeolian dust flux increased markedly over the SO as well as Antarctica (e.g., Lambert et al., 2008; Martínez-Garcia et al., 2011). Increased marine productivity stimulated by the increased dust flux (Fe fertilization) is thought to have occurred in the Subantarctic Zone (e.g., Jaccard et al., 2013; Martínez-Garcia et al., 2014; Struve et al., 2020), which falls in the latitude band of the major Southern Hemisphere dust sources and their wind path (Fig. 1) (Watson et al., 2000; Sigman et al., 2010). Indeed, Yamazaki and Ikehara (2012) have proposed that Fe fertilization enhanced the production of biogenic magnetite, which in turn controls the MS signal, at the MR03K04-PC5 site. The abundance of terrigenous component also increased during glacial periods (Yamazaki and Ikehara, 2012). Thus, we suggest that Fe fertilization played an important role, especially during the first half of MIS 6. This mechanism can explain the increased MS in the MR03K04-PC5 core in the Subantarctic Zone but not in the DCR-1PC core in the Antarctic Zone, although it cannot explain why Fe fertilization played the role only during the first half of MIS 6. We also found an increased dust proxy signal during the first half of MIS 6 (~190–170 ka) in the PS75/59-2 core (Lamy et al., 2014) from the Pacific sector (Fig. 6). The PS75/59-2 site is located ~2° and ~4° north of the modern SAF and PF, respectively (Park et al., 2019) (Fig. 1a), and its lithology is primarily foraminifera-bearing calcareous nannofossil ooze containing minor amounts of diatoms (Gersonde, 2011; Lamy et al., 2014). We infer that the PS75/59-2 core site would have been located in the Subantarctic Zone during past glacial periods, recording a dust proxy signal similar to that of the MR03K04-PC5 core during the first half of MIS 6. However, the PS75/56-1 core, which relative positions to the fronts are similar to the PS75/59-2 core (Park et al., 2019) (Fig. 1a), did not show an increased dust proxy signal during the first half of MIS 6 (Fig. 6). The dominant lithologies of International Ocean Discovery Program (IODP) Site U1540 core (a counterpart to the PS75/56-1 core) and IODP Site U1541 core (a counterpart to the PS75/59-2 core) are diatom ooze and calcareous ooze, respectively (Winckler et al., 2021), which implies that the PS75/56-1 site was located in the Antarctic Zone during past glacial periods. Therefore, understanding the role of Fe fertilization in dust proxy signals will contribute to establishing more reliable dust correlation in the circum-Antarctic SO.

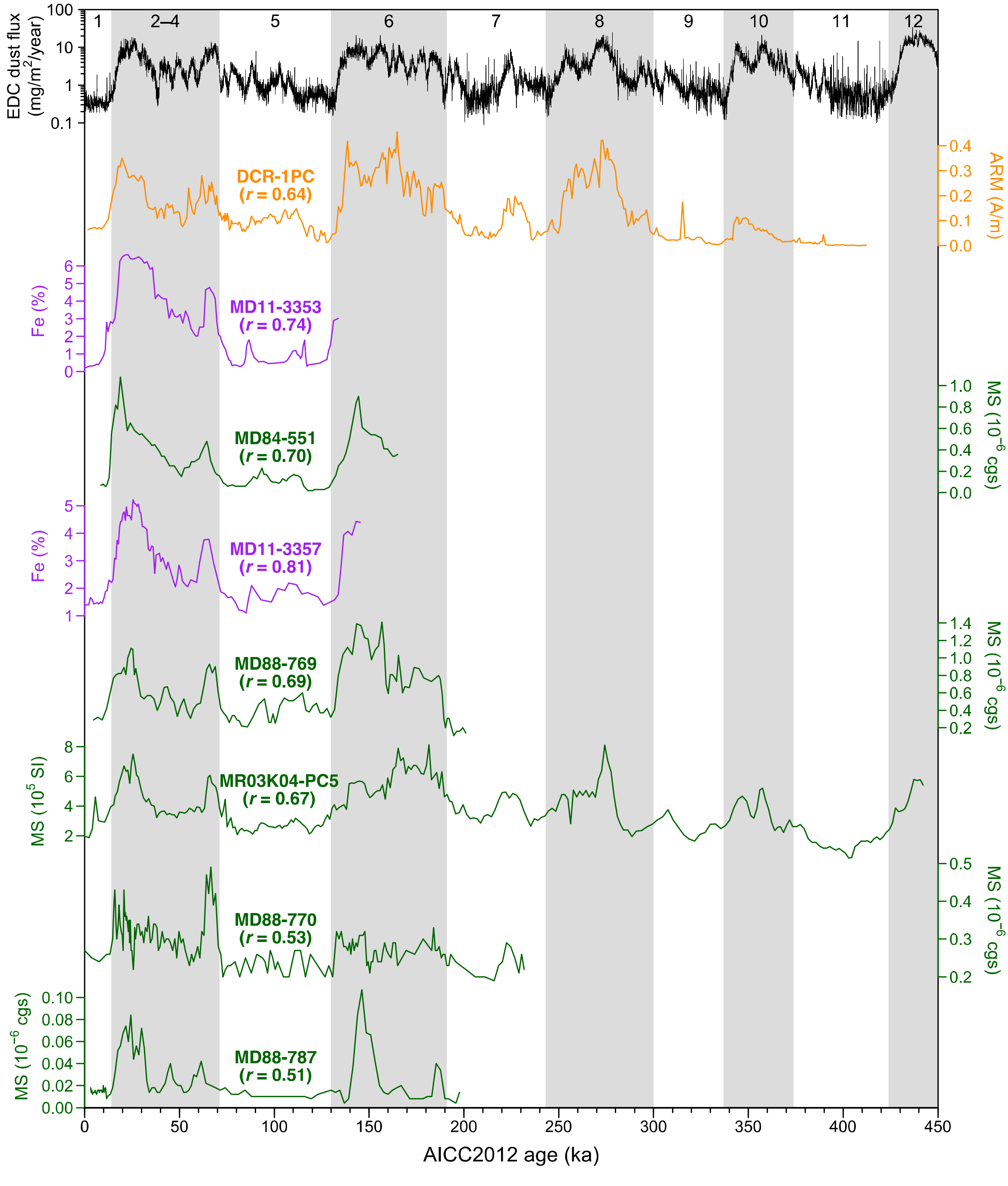

Fig. 5. Dust proxy signals at eight sites in the Indian sector of the Southern Ocean (locations of the sites are provided in Fig. 1b and Table 1). All the dust proxy signals (Bareille et al., 1994; Yamazaki and Ikehara, 2012; Thöle et al., 2019; this study) were matched to the EDC dust flux (Lambert et al., 2012) using the Match program (Lisiecki and Lisiecki, 2002). The correlation coefficients (*r*) between the dust proxy signals at each site with the EDC dust flux

are also shown. Glacial intervals are indicated by gray bars.

5.3. Sector-scale variations in dust proxy records

Dust correlation provides a means to construct age–depth models in the SO on glacial–interglacial timescales (Pugh et al., 2009; this study) and has been applied to millennial timescales for cores from the Atlantic sector (Weber et al., 2012, 2014; Anderson et al., 2014). However, neither the difference in dust proxy signals between the three sectors of the SO (Indian, Pacific, and Atlantic) nor the difference in dust proxy signals between past glacial periods have been investigated in detail. Here we compiled 20 dust proxy records (including the DCR-1PC core) from the three sectors of the SO over the last 450 kyrs (Fig. 6; Table 1) and assessed any differences in terms of the correlation coefficients with the EDC dust flux (Lambert et al., 2012). The average sampling resolution is generally high (< 1 kyr) for the sites in the Pacific and Atlantic sectors, but low (> 1 kyr) in the Indian sector (Table 1).

Linear correlation coefficients for the last 450 kyrs between the marine sediment-core dust proxy signals (linear scale, resampled every 1 kyr) based on the dust age models and the EDC dust flux (log scale) are 0.62–0.78 in the Pacific sector (169°W to 114°W, 54°S to 60°S) and 0.70–0.90 in the Atlantic sector (43°W to 8°E, 42°S to 59°S) (Table 2). Comparing also with the Indian sector ($0.51 < r < 0.81$; Table 2), it is clear that the correlation coefficient is strongest in the Atlantic sector. Although the age ranges of the MD07-3133, MD07-3134, and PS2498-1 cores in the Atlantic sector are narrower than of the other considered cores, the linear correlation coefficients for the last 100 kyrs still exhibit stronger correlation in the Atlantic sector (0.71–0.90) than in the Pacific sector (0.58–0.84) or the Indian sector (0.55–0.77) (Table 2). Thus, the marine sediment-core dust proxy signals in the Atlantic sector are most comparable to the EDC dust flux.

We computed moving correlation coefficients between the marine sediment-core dust proxy signals (linear scale) and the EDC dust flux (log scale) with a 10-kyr window using the package '*astrochron*' (Meyers, 2014) in the *R* environment (R core team, 2021), after each record had been resampled every 1 kyr and normalized to have zero mean and one standard deviation (Fig. 6). Large variabilities in the correlation coefficients are apparent at each site over the last 450 kyrs (Fig. 6), regardless of the choice of linear or log scale of the marine sediment-core dust proxy signals and the EDC dust flux.

To examine the common features of the moving correlation coefficients at multiple sites, we computed the arithmetic means of the correlation coefficients in turn for all 20 sites (Fig. 7a) and for each sector of the SO (Fig. 7b–7d). We found that the averaged moving correlation of all 20 sites is generally strong for the glacial periods and weak for the interglacial periods (Fig. 7a). Importantly, the correlation is strong (weak) when the EDC dust flux was high (low), which suggests that increased dust input from dust sources to the Antarctic ice core also allowed the SO marine sediments to preserve the comparable dust proxy signals. An exception occurred, however, during the first half of MIS 6 (~185–160 ka), when the correlation is weak but the EDC dust flux was relatively high and variable (Fig. 7a). Although some effect of Fe fertilization on the dust proxy signals in the Indian sector during MIS 6 is expected (Fig. 5) (see Section 5.2), the weak correlation in the Pacific and Atlantic sectors (e.g., the PS75/59-2 and ODP Site 1090 cores) (Figs. 6, 7) implies a common controlling factor.

We also considered the average moving correlation in each sector of the SO (Fig. 7b–7d). In spite of the small number of records (fewer than four) in the Indian sector beyond 200 ka (Fig. 7e), the averages of the Indian and Pacific sectors roughly follow the average of all 20 sites over the last 450 kyrs (Fig. 7b, c). According to Lamy et al. (2014), large-scale climate forcings such as westerlies and glaciogenic dust mobilization are thought to control the dust proxy signals in the Pacific and Atlantic sectors. Thus, the similarity of the correlation coefficients between the Indian and Pacific sectors can be explained by the same forcing mechanisms having controlled the dust proxy signals in the Indian sector. The low average correlation coefficients in the Atlantic sector during MIS 8 (~300–265 ka) and MIS 6 (~190–165 ka) (Fig. 7d) may largely reflect variable dust proxy signal at ODP Site 1094 in the Antarctic Zone (Figs. 1a, 6), which would have been influenced by volcanic material from the South Sandwich Islands and by the glacial sea-ice extent (Latimer et al., 2006). Previous study at ODP Site 1094 indicated that MS signal is generally similar to the variability of ice rafted debris (predominantly ash), and that the ash originated principally from South Sandwich Islands is transported by sea ice and icebergs (Kanfoush et al., 2002). In contrast, the correlation coefficients at ODP Site 1090 in the Subantarctic Zone (Figs. 1a, 6) are similar to the average of all 20 sites during MIS 8 and MIS 6 (Fig. 7a). We also note the difference in the average sampling resolution between ODP Site 1094 (> 1 kyr) and ODP Site 1090 (< 1 kyr) (Table 1). Overall, large-scale climate forcings (westerlies, glaciogenic dust mobilization, and wind-driven current transport) likely controlled the dust proxy signals in all three sectors of the SO over the last 450 kyrs.

For the interval representing the last ~150 kyrs, the average correlation coefficients for the Indian sector are somewhat lower in some intervals (e.g., 95–83 ka and 51–43 ka) than for the Pacific and Atlantic sectors (Fig. 7). Considering that the dominant dust source for the EDC site was South America during MIS 2 and 4 (e.g., Delmonte et al., 2004, 2008; Oyabu et al., 2020) and possibly Australia during MIS 5e (Revel-Rolland et al., 2006), the low correlation coefficients in the Indian sector imply contributions of dust from South Africa and volcanic materials from the Crozet and Kerguelen Plateaus, to the Indian sector (e.g., Bareille et al., 1994; Thöle et al., 2019). The low average sampling resolution (> 1 kyr) (Table 1) may also partly explain the low correlation coefficients. Thus, much caution is needed in applying dust correlation in the Indian sector of the SO, at least over the last ~150 kyrs, especially for precise lead and lag analyses within a few kiloyears. More records of dust proxy signals in the Indian sector beyond the last ~150 kyrs with sufficient sampling resolution (i.e., < 1 kyr) will contribute to detailed comparisons with the dust proxy signals in the Pacific and Atlantic sectors of the SO, facilitating widening and strengthening of the application of dust correlation in the circum-Antarctic ocean for the purpose of constructing a robust chronology.

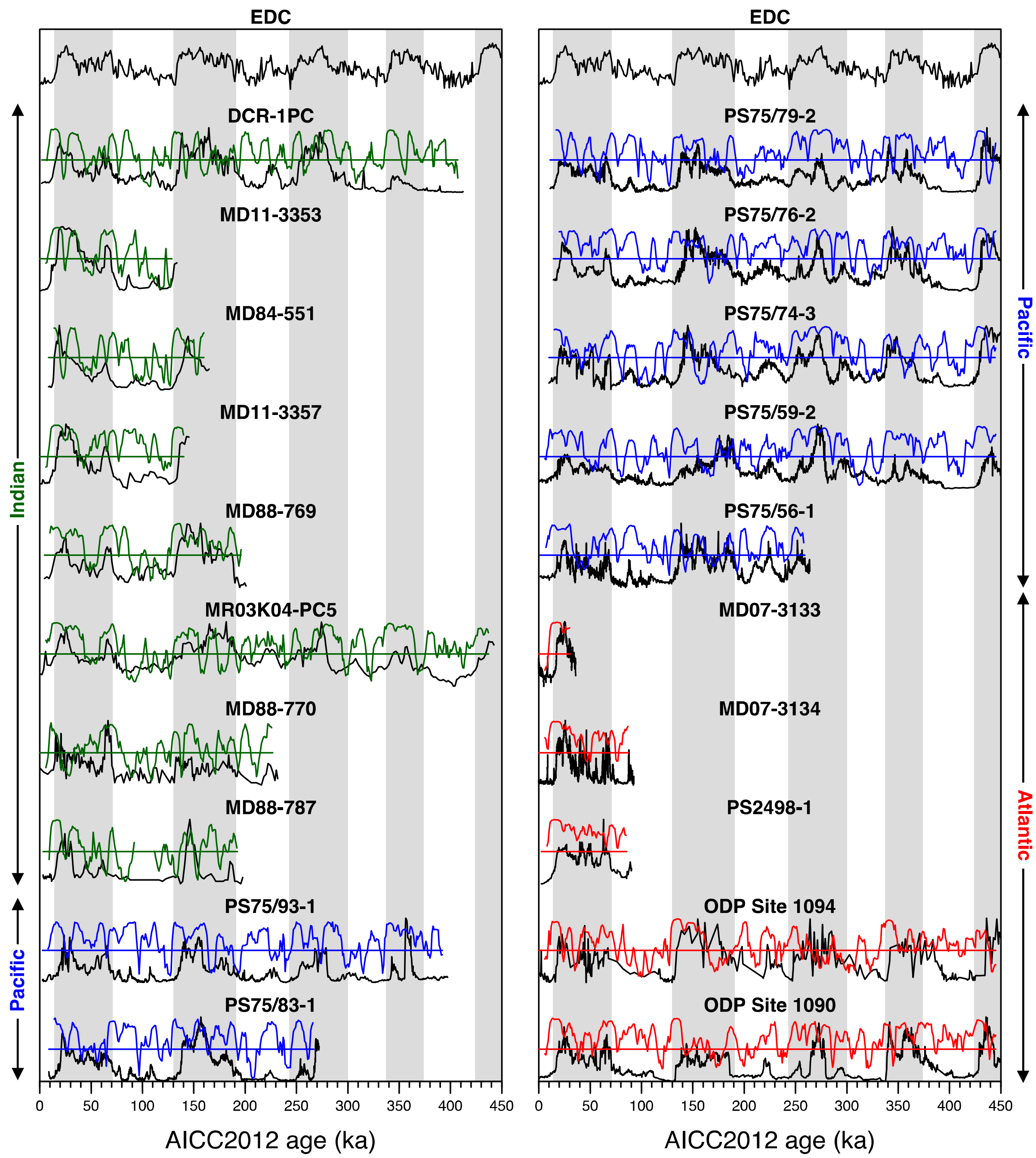

Fig. 6. Compilation of dust proxy records in the Southern Ocean over the last 450 kyrs (the

locations of the sites are provided in Fig. 1a and Table 1). Colored lines (green: Indian sector; blue: Pacific sector; red: Atlantic sector) indicate moving correlation coefficients between each dust proxy signal and the EDC dust flux (Lambert et al., 2012) on the AICC2012 timescale (Veres et al., 2013; Bazin et al., 2013). Colored horizontal lines are zero values of correlation coefficients. Positive (negative) values of correlation coefficients indicate that each dust proxy signal is positively (negatively) correlated with the EDC dust flux. Moving correlation was computed for a 10-kyr window after each record was resampled every 1 kyr and normalized. Glacial intervals are indicated by gray bars.

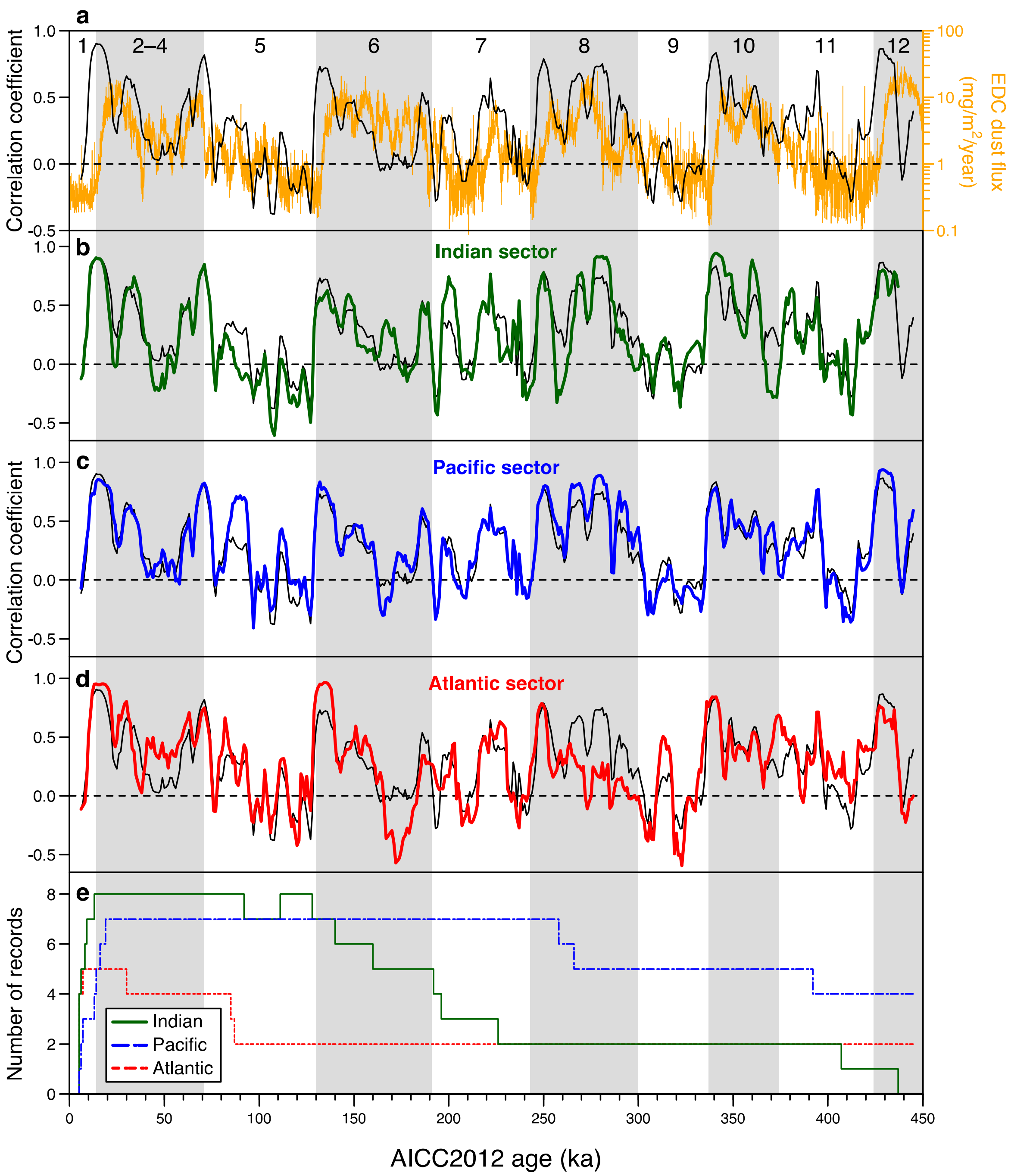

Fig. 7. Averages of moving correlation coefficients between each dust proxy signal and the EDC dust flux (Lambert et al., 2012) on the AICC2012 timescale (Veres et al., 2013; Bazin et al., 2013). (a) Average of all 20 sites (black line) and the EDC dust flux (orange line). (b–d) Averages of the sites in the three sectors (green: Indian; blue: Pacific; red: Atlantic). The average of all sites (black line) is also shown. (e) Number of records in each sector. Glacial intervals are indicated by gray bars.

6. Conclusions

We conducted a direct comparison of the ^{14}C ages, δD–SST alignment, $\delta^{18}O$ stratigraphy, and dust correlation for the DCR-1PC core to assess the reliability of dust correlation in the Indian sector of the SO. We found consistency between the $\delta^{18}O$ stratigraphy and dust correlation within uncertainty, confirming the reliability of the latter chronology for glacial–interglacial timescales in the Indian sector, at least over the last ~410 kyrs. However, the dust correlation tends to show older ages than the $\delta^{18}O$ stratigraphy by up to 3 kyrs. We also compared the dust proxy signals in the DCR-1PC core with available dust proxy records from the Indian sector of the SO, and we found a marked difference for MIS 6 between the DCR-1PC and MR03K04-PC5 cores. Considering the positions of the two cores relative to the oceanic fronts during past glacial periods, we suggest that iron fertilization may have played an important role in modulating the magnetic signal at the MR03K04-PC5 site in the Subantarctic Zone, but not at the DCR-1PC site in the Antarctic Zone. We further compiled dust proxy records from the Pacific and Atlantic sectors of the SO to assess the differences in the dust proxy signals between the sectors and to determine the sector-scale variations in the dust proxy records over the last 450 kyrs. The linear correlation coefficients between the marine sediment-core dust proxy signals and the EDC dust flux are strongest in the Atlantic sector. In turn, moving correlation coefficients between the marine sediment-core dust proxy signals and the EDC dust flux indicate a strong correlation for times of high EDC dust flux, except for MIS 6. Although the differences in the moving correlations between the three sectors are minor, implying dominant control by large-scale climate forcings such as westerlies and glaciogenic dust mobilization, the correlation in the Indian sector is slightly lower than in the other sectors for the last ~150 kyrs. The low correlation possibly reflects the contribution of dust from South Africa and volcanic materials from the Crozet and Kerguelen Plateaus; hence, we caution against applying dust correlation in the Indian sector of the SO for precise lead and lag analyses within a few kiloyears.

Acknowledgments

We would like to thank Y. Fujimura, T. Minami, and H. Wakaki-Uchimura for their support during the stable isotope measurements of the DCR-1PC core. We also thank T. Yamazaki for providing access to the magnetic susceptibility data of the MR03K04-PC5 core, and X. Crosta, E. Michel, H.E. Amsler, M. Civel-Mazens, H. Asahi, Y. Kato, and the members of the research project “Giant Reservoirs – Antarctic” for helpful suggestions about marine sediment-core and ice core chronologies. We are grateful to the scientists and crew of the *Hakuho-maru* KH-10-7 Cruise for the initial data collection of the DCR-1PC core. All the figures were plotted using R and GMT software. The manuscript was improved by constructive comments from the editor (I. Hendy) and two anonymous reviewers. This work was supported by the Japan Society for the Promotion of Science KAKENHI (Grants-in-Aid for Scientific Research) [grant numbers 17H06318 to MI and OS, 17H06320 to KK, and 17H06321 to YS]. Supporting data are included as three tables in the supporting information files; any additional data may be obtained from H.M. (email: hmatsui@gipc.akita-u.ac.jp).

References

Anderson, R.F., Barker, S., Fleisher, M., Gersonde, R., Goldstein, S.L., Kuhn, G., Mortyn, P.G., Pahnke, K., Sachs, J.P., 2014. Biological response to millennial variability of dust and nutrient supply in the Subantarctic South Atlantic Ocean. Philosophical Transactions of the Royal Society A: Mathematical, Physical and Engineering Sciences 372, 20130054. https://doi.org/10.1098/rsta.2013.0054

Bareille, G., Grousset, F.E., Labracherie, M., Labeyrie, L.D., Petit, J.-R., 1994. Origin of detrital fluxes in the southeast Indian Ocean during the last climatic cycles.

Paleoceanography 9, 799–819. https://doi.org/10.1029/94PA01946

Basile, I., Grousset, F.E., Revel, M., Petit, J.R., Biscaye, P.E., Barkov, N.I., 1997. Patagonian origin of glacial dust deposited in East Antarctica (Vostok and Dome C) during glacial stages 2, 4 and 6. Earth and Planetary Science Letters 146, 573–589. https://doi.org/10.1016/S0012-821X(96)00255-5

Bazin, L., Landais, A., Lemieux-Dudon, B., Toyé Mahamadou Kele, H., Veres, D., Parrenin, F., Martinerie, P., Ritz, C., Capron, E., Lipenkov, V., Loutre, M.-F., Raynaud, D., Vinther, B., Svensson, A., Rasmussen, S.O., Severi, M., Blunier, T., Leuenberger, M., Fischer, H., Masson-Delmotte, V., Chappellaz, J., Wolff, E., 2013. An optimized multi-proxy, multi-site Antarctic ice and gas orbital chronology (AICC2012): 120–800 ka. Clim. Past 9, 1715–1731. https://doi.org/10.5194/cp-9-1715-2013

Burckle, L.H., Cirilli, J., 1987. Origin of diatom ooze belt in the Southern Ocean: Implications for late Quaternary paleoceanography. Micropaleontology 33, 82–86. https://doi.org/10.2307/1485529

Channell, J.E.T., Xuan, C., Hodell, D.A., 2009. Stacking paleointensity and oxygen isotope data for the last 1.5 Myr (PISO-1500). Earth and Planetary Science Letters 283, 14–23. https://doi.org/10.1016/j.epsl.2009.03.012

Civel-Mazens, M., Crosta, X., Cortese, G., Michel, E., Mazaud, A., Ther, O., Ikehara, M., Itaki, T., 2021. Impact of the Agulhas Return Current on the oceanography of the Kerguelen Plateau region, Southern Ocean, over the last 40 kyrs. Quaternary Science Reviews 251, 106711. https://doi.org/10.1016/j.quascirev.2020.106711

Crosta, X., Shukla, S.K., Ther, O., Ikehara, M., Yamane, M., Yokoyama, Y., 2020. Last Abundant Appearance Datum of *Hemidiscus karstenii* driven by climate change. Marine Micropaleontology 157, 101861. https://doi.org/10.1016/j.marmicro.2020.101861

Delmonte, B., Basile-Doelsch, I., Petit, J.-R., Maggi, V., Revel-Rolland, M., Michard, A., Jagoutz, E., Grousset, F., 2004. Comparing the Epica and Vostok dust records during the last 220,000 years: stratigraphical correlation and provenance in glacial periods. Earth-Science Reviews 66, 63–87. https://doi.org/10.1016/j.earscirev.2003.10.004

Delmonte, B., Andersson, P.S., Hansson, M., Schöberg, H., Petit, J.R., Basile-Doelsch, I., Maggi, V., 2008. Aeolian dust in East Antarctica (EPICA-Dome C and Vostok): Provenance during glacial ages over the last 800 kyr. Geophysical Research Letters 35. https://doi.org/10.1029/2008GL033382

Dezileau, L., Bareille, G., Reyss, J.L., Lemoine, F., 2000. Evidence for strong sediment redistribution by bottom currents along the southeast Indian ridge. Deep Sea Research Part I: Oceanographic Research Papers 47, 1899–1936. https://doi.org/10.1016/S0967-0637(00)00008-X

Diekmann, B., 2007. Sedimentary patterns in the late Quaternary Southern Ocean. Deep Sea Research Part II: Topical Studies in Oceanography 54, 2350–2366. https://doi.org/10.1016/j.dsr2.2007.07.025

Duplessy, J.-C., Shackleton, N.J., Matthews, R.K., Prell, W., Ruddiman, W.F., Caralp, M., Hendy, C.H., 1984. ^{13}C Record of benthic foraminifera in the last interglacial ocean: Implications for the carbon cycle and the global deep water circulation. Quaternary Research 21, 225–243. https://doi.org/10.1016/0033-5894(84)90099-1

Elderfield, H., Ferretti, P., Greaves, M., Crowhurst, S., McCave, I.N., Hodell, D., Piotrowski, A.M., 2012. Evolution of Ocean Temperature and Ice Volume Through the Mid-Pleistocene Climate Transition. Science 337, 704–709. https://doi.org/10.1126/science.1221294

Gersonde, R., 2011. The expedition of the research vessel "Polarstern" to the polar South Pacific in 2009/2010 (ANT-XXVI/2 - BIPOMAC), Berichte zur Polar- und Meeresforschung (Rep. Polar Marine Res.), Bremerhaven, Alfred Wegener Institute for

Polar and Marine Research, 632, 330. https://doi.org/10.2312/BzPM_0632_2011
Gersonde, R., Abelmann, A., Brathauer, U., Becquey, S., Bianchi, C., Cortese, G., Grobe, H., Kuhn, G., Niebler, H.-S., Segl, M., Sieger, R., Zielinski, U., Fütterer, D.K., 2003. Last glacial sea surface temperatures and sea-ice extent in the Southern Ocean (Atlantic-Indian sector): A multiproxy approach. Paleoceanography 18, 1061. https://doi.org/10.1029/2002PA000809
Gersonde, R., Crosta, X., Abelmann, A., Armand, L., 2005. Sea-surface temperature and sea ice distribution of the Southern Ocean at the EPILOG Last Glacial Maximum—a circum-Antarctic view based on siliceous microfossil records. Quaternary Science Reviews 24, 869–896. https://doi.org/10.1016/j.quascirev.2004.07.015
Govin, A., Michel, E., Labeyrie, L., Waelbroeck, C., Dewilde, F., Jansen, E., 2009. Evidence for northward expansion of Antarctic Bottom Water mass in the Southern Ocean during the last glacial inception. Paleoceanography 24, PA1202. https://doi.org/10.1029/2008PA001603
Govin, A., Capron, E., Tzedakis, P.C., Verheyden, S., Ghaleb, B., Hillaire-Marcel, C., St-Onge, G., Stoner, J.S., Bassinot, F., Bazin, L., Blunier, T., Combourieu-Nebout, N., El Ouahabi, A., Genty, D., Gersonde, R., Jimenez-Amat, P., Landais, A., Martrat, B., Masson-Delmotte, V., Parrenin, F., Seidenkrantz, M.-S., Veres, D., Waelbroeck, C., Zahn, R., 2015. Sequence of events from the onset to the demise of the Last Interglacial: Evaluating strengths and limitations of chronologies used in climatic archives. Quaternary Science Reviews 129, 1–36. https://doi.org/10.1016/j.quascirev.2015.09.018
Hasenfratz, A.P., Jaccard, S.L., Martínez-García, A., Sigman, D.M., Hodell, D.A., Vance, D., Bernasconi, S.M., Kleiven, H. (Kikki) F., Haumann, F.A., Haug, G.H., 2019. The residence time of Southern Ocean surface waters and the 100,000-year ice age cycle.

Science 363, 1080–1084. https://doi.org/10.1126/science.aat7067

Hayes, C.T., Martínez-García, A., Hasenfratz, A.P., Jaccard, S.L., Hodell, D.A., Sigman, D.M., Haug, G.H., Anderson, R.F., 2014. A stagnation event in the deep South Atlantic during the last interglacial period. Science 346, 1514. https://doi.org/10.1126/science.1256620

Horiuchi, K., Kamata, K., Maejima, S., Sasaki, S., Sasaki, N., Yamazaki, T., Fujita, S., Motoyama, H., Matsuzaki, H., 2016. Multiple ^{10}Be records revealing the history of cosmic-ray variations across the Iceland Basin excursion. Earth and Planetary Science Letters 440, 105–114. https://doi.org/10.1016/j.epsl.2016.01.034

Itaki, T., Taira, Y., Kuwamori, N., Saito, H., Ikehara, M., Hoshino, T., 2020. Innovative microfossil (radiolarian) analysis using a system for automated image collection and AI-based classification of species. Sci Rep 10, 21136. https://doi.org/10.1038/s41598-020-77812-6

Jaccard, S.L., Hayes, C.T., Martínez-Garcia, A., Hodell, D.A., Anderson, R.F., Sigman, D.M., Haug, G.H., 2013. Two Modes of Change in Southern Ocean Productivity Over the Past Million Years. Science 339, 1419–1423. https://doi.org/10.1126/science.1227545

Jouzel, J., Masson-Delmotte, V., Cattani, O., Dreyfus, G., Falourd, S., Hoffmann, G., Minster, B., Nouet, J., Barnola, J.M., Chappellaz, J., Fischer, H., Gallet, J.C., Johnsen, S., Leuenberger, M., Loulergue, L., Luethi, D., Oerter, H., Parrenin, F., Raisbeck, G., Raynaud, D., Schilt, A., Schwander, J., Selmo, E., Souchez, R., Spahni, R., Stauffer, B., Steffensen, J.P., Stenni, B., Stocker, T.F., Tison, J.L., Werner, M., Wolff, E.W., 2007. Orbital and Millennial Antarctic Climate Variability over the Past 800,000 Years. Science 317, 793–796. https://doi.org/10.1126/science.1141038

Kanfoush, S.L., Hodell, D.A., Charles, C.D., Janecek, T.R., Rack, F.R., 2002. Comparison of ice-rafted debris and physical properties in ODP Site 1094 (South Atlantic) with the

Vostok ice core over the last four climatic cycles. Palaeogeography, Palaeoclimatology, Palaeoecology 182, 329–349. https://doi.org/10.1016/S0031-0182(01)00502-8

Kawamura, K., Parrenin, F., Lisiecki, L., Uemura, R., Vimeux, F., Severinghaus, J.P., Hutterli, M.A., Nakazawa, T., Aoki, S., Jouzel, J., Raymo, M.E., Matsumoto, K., Nakata, H., Motoyama, H., Fujita, S., Goto-Azuma, K., Fujii, Y., Watanabe, O., 2007. Northern Hemisphere forcing of climatic cycles in Antarctica over the past 360,000 years. Nature 448, 912–916. https://doi.org/10.1038/nature06015

Kim, S., Yoo, K.-C., Lee, J.I., Lee, M.K., Kim, K., Yoon, H.I., Moon, H.S., 2018. Relationship between magnetic susceptibility and sediment grain size since the last glacial period in the Southern Ocean off the northern Antarctic Peninsula – Linkages between the cryosphere and atmospheric circulation. Palaeogeography, Palaeoclimatology, Palaeoecology 505, 359–370. https://doi.org/10.1016/j.palaeo.2018.06.016

Kohfeld, K.E., Graham, R.M., de Boer, A.M., Sime, L.C., Wolff, E.W., Le Quéré, C., Bopp, L., 2013. Southern Hemisphere westerly wind changes during the Last Glacial Maximum: paleo-data synthesis. Quaternary Science Reviews 68, 76–95. https://doi.org/10.1016/j.quascirev.2013.01.017

Labeyrie, L., Labracherie, M., Gorfti, N., Pichon, J.J., Vautravers, M., Arnold, M., Duplessy, J.-C., Paterne, M., Michel, E., Duprat, J., Caralp, M., Turon, J.-L., 1996. Hydrographic changes of the Southern Ocean (southeast Indian Sector) Over the last 230 kyr. Paleoceanography 11, 57–76. https://doi.org/10.1029/95PA02255

Lambert, F., Delmonte, B., Petit, J.R., Bigler, M., Kaufmann, P.R., Hutterli, M.A., Stocker, T.F., Ruth, U., Steffensen, J.P., Maggi, V., 2008. Dust-climate couplings over the past 800,000 years from the EPICA Dome C ice core. Nature 452, 616–619. https://doi.org/10.1038/nature06763

Lambert, F., Bigler, M., Steffensen, J.P., Hutterli, M., Fischer, H., 2012. Centennial mineral dust variability in high-resolution ice core data from Dome C, Antarctica. Clim. Past 8, 609–623. https://doi.org/10.5194/cp-8-609-2012

Lamy, F., Gersonde, R., Winckler, G., Esper, O., Jaeschke, A., Kuhn, G., Ullermann, J., Martínez-Garcia, A., Lambert, F., Kilian, R., 2014. Increased Dust Deposition in the Pacific Southern Ocean During Glacial Periods. Science 343, 403–407. https://doi.org/10.1126/science.1245424

Latimer, J.C., Filippelli, G.M., Hendy, I.L., Gleason, J.D., Blum, J.D., 2006. Glacial-interglacial terrigenous provenance in the southeastern Atlantic Ocean: The importance of deep-water sources and surface currents. Geology 34, 545-548. https://doi.org/10.1130/G22252.1

Li, F., Ginoux, P., Ramaswamy, V., 2008. Distribution, transport, and deposition of mineral dust in the Southern Ocean and Antarctica: Contribution of major sources. J. Geophys. Res. 113, D10207. https://doi.org/10.1029/2007JD009190

Li, F., Ramaswamy, V., Ginoux, P., Broccoli, A.J., Delworth, T., Zeng, F., 2010. Toward understanding the dust deposition in Antarctica during the Last Glacial Maximum: Sensitivity studies on plausible causes. J. Geophys. Res. 115. https://doi.org/10.1029/2010JD014791

Lisiecki, L.E., Lisiecki, P.A., 2002. Application of dynamic programming to the correlation of paleoclimate records. Paleoceanography 17, 1049. https://doi.org/10.1029/2001PA000733

Lisiecki, L.E., Raymo, M.E., 2005. A Pliocene-Pleistocene stack of 57 globally distributed benthic $\delta^{18}O$ records. Paleoceanography 20, PA1003. https://doi.org/10.1029/2004PA001071

Lougheed, B.C., Metcalfe, B., Ninnemann, U.S., Wacker, L., 2018. Moving beyond the age–

depth model paradigm in deep-sea palaeoclimate archives: dual radiocarbon and stable isotope analysis on single foraminifera. Clim. Past 14, 515–526. https://doi.org/10.5194/cp-14-515-2018

Löwemark, L., Grootes, P.M., 2004. Large age differences between planktic foraminifers caused by abundance variations and *Zoophycos* bioturbation. Paleoceanography 19. https://doi.org/10.1029/2003PA000949

Martínez-Garcia, A., Rosell-Melé, A., Jaccard, S.L., Geibert, W., Sigman, D.M., Haug, G.H., 2011. Southern Ocean dust–climate coupling over the past four million years. Nature 476, 312–315. https://doi.org/10.1038/nature10310

Martínez-García, A., Sigman, D.M., Ren, H., Anderson, R.F., Straub, M., Hodell, D.A., Jaccard, S.L., Eglinton, T.I., Haug, G.H., 2014. Iron Fertilization of the Subantarctic Ocean During the Last Ice Age. Science 343, 1347–1350. https://doi.org/10.1126/science.1246848

Mazaud, A., Sicre, M.A., Ezat, U., Pichon, J.J., Duprat, J., Laj, C., Kissel, C., Beaufort, L., Michel, E., Turon, J.L., 2002. Geomagnetic-assisted stratigraphy and sea surface temperature changes in core MD94-103 (Southern Indian Ocean): possible implications for North–South climatic relationships around H4. Earth and Planetary Science Letters 201, 159–170. https://doi.org/10.1016/S0012-821X(02)00662-3

Meyers, S.R., 2014. Astrochron: An R Package for Astrochronology (Version 1.0). https://cran.r-project.org/package=astrochron

Ohgaito, R., Abe-Ouchi, A., O'ishi, R., Takemura, T., Ito, A., Hajima, T., Watanabe, S., Kawamiya, M., 2018. Effect of high dust amount on surface temperature during the Last Glacial Maximum: a modelling study using MIROC-ESM. Clim. Past 14, 1565–1581. https://doi.org/10.5194/cp-14-1565-2018

Orsi, A.H., Whitworth, T., Nowlin, W.D., 1995. On the meridional extent and fronts of the

Antarctic Circumpolar Current. Deep Sea Research Part I: Oceanographic Research Papers 42, 641–673. https://doi.org/10.1016/0967-0637(95)00021-W

Oyabu, I., Iizuka, Y., Kawamura, K., Wolff, E., Severi, M., Ohgaito, R., Abe-Ouchi, A., Hansson, M., 2020. Compositions of Dust and Sea Salts in the Dome C and Dome Fuji Ice Cores From Last Glacial Maximum to Early Holocene Based on Ice-Sublimation and Single-Particle Measurements. J. Geophys. Res. Atmos. 125. https://doi.org/10.1029/2019JD032208

Park, Y. -H., Park, T., Kim, T. -W., Lee, S. -H., Hong, C. -S., Lee, J. -H., Rio, M. -H., Pujol, M. -I., Ballarotta, M., Durand, I., Provost, C., 2019. Observations of the Antarctic Circumpolar Current Over the Udintsev Fracture Zone, the Narrowest Choke Point in the Southern Ocean. J. Geophys. Res. Oceans 2019JC015024. https://doi.org/10.1029/2019JC015024

Past Interglacials Working Group of PAGES, 2016. Interglacials of the last 800,000 years. Reviews of Geophysics 54, 162–219. https://doi.org/10.1002/2015RG000482

Petit, J.R., Mourner, L., Jouzel, J., Korotkevich, Y.S., Kotlyakov, V.I., Lorius, C., 1990. Palaeoclimatological and chronological implications of the Vostok core dust record. Nature 343, 56–58. https://doi.org/10.1038/343056a0

Pugh, R.S., McCave, I.N., Hillenbrand, C.-D., Kuhn, G., 2009. Circum-Antarctic age modelling of Quaternary marine cores under the Antarctic Circumpolar Current: Ice-core dust–magnetic correlation. Earth and Planetary Science Letters 284, 113–123. https://doi.org/10.1016/j.epsl.2009.04.016

R Core Team, 2021. R: A language and environment for statistical computing. R Foundation for Statistical Computing, Vienna, Austria. https://www.R-project.org/.

Revel-Rolland, M., De Deckker, P., Delmonte, B., Hesse, P.P., Magee, J.W., Basile-Doelsch, I., Grousset, F., Bosch, D., 2006. Eastern Australia: A possible source of dust in East

Antarctica interglacial ice. Earth and Planetary Science Letters 249, 1–13. https://doi.org/10.1016/j.epsl.2006.06.028

Sakamoto, T., Kuroki, K., Sugawara, T., Aoike, K., Iijima, K., Sugisaki, S., 2006. Non-Destructive X-Ray Fluorescence (XRF) Core-Imaging Scanner, TATSCAN-F2. Sci. Dril. 2, 37–39. https://doi.org/10.5194/sd-2-37-2006

Sarmiento, J.L., Gruber, N., Brzezinski, M.A., Dunne, J.P., 2004. High-latitude controls of thermocline nutrients and low latitude biological productivity. Nature 427, 56–60. https://doi.org/10.1038/nature02127

Shukla, S.K., Crosta, X., Ikehara, M., 2021. Sea Surface Temperatures in the Indian Sub-Antarctic Southern Ocean for the Last Four Interglacial Periods. Geophysical Research Letters 48, e2020GL090994. https://doi.org/10.1029/2020GL090994

Sigman, D.M., Hain, M.P., Haug, G.H., 2010. The polar ocean and glacial cycles in atmospheric CO_2 concentration. Nature 466, 47–55. https://doi.org/10.1038/nature09149

Stern, J.V., Lisiecki, L.E., 2014. Termination 1 timing in radiocarbon-dated regional benthic $\delta^{18}O$ stacks. Paleoceanography 29, 1127–1142. https://doi.org/10.1002/2014PA002700

Stoner, J.S., St-Onge, G., 2007. Chapter Three Magnetic Stratigraphy in Paleoceanography: Reversals, Excursions, Paleointensity, and Secular Variation, in: Hillaire–Marcel, C., De Vernal, A. (Eds.), Developments in Marine Geology. Elsevier, pp. 99–138. https://doi.org/10.1016/S1572-5480(07)01008-1

Stoner, J.S., Channell, J.E.T., Hillaire-Marcel, C., Kissel, C., 2000. Geomagnetic paleointensity and environmental record from Labrador Sea core MD95-2024: global marine sediment and ice core chronostratigraphy for the last 110 kyr. Earth and Planetary Science Letters 183, 161–177. https://doi.org/10.1016/S0012-821X(00)00272-7

Struve, T., Pahnke, K., Lamy, F., Wengler, M., Böning, P., Winckler, G., 2020. A circumpolar dust conveyor in the glacial Southern Ocean. Nat Commun 11, 5655. https://doi.org/10.1038/s41467-020-18858-y

Suganuma, Y., Yokoyama, Y., Yamazaki, T., Kawamura, K., Horng, C.-S., Matsuzaki, H., 2010. 10Be evidence for delayed acquisition of remanent magnetization in marine sediments: Implication for a new age for the Matuyama–Brunhes boundary. Earth and Planetary Science Letters 296, 443–450. https://doi.org/10.1016/j.epsl.2010.05.031

Thöle, L.M., Amsler, H.E., Moretti, S., Auderset, A., Gilgannon, J., Lippold, J., Vogel, H., Crosta, X., Mazaud, A., Michel, E., Martínez-García, A., Jaccard, S.L., 2019. Glacial-interglacial dust and export production records from the Southern Indian Ocean. Earth and Planetary Science Letters 525, 115716. https://doi.org/10.1016/j.epsl.2019.115716

Ullermann, J., Lamy, F., Ninnemann, U., Lembke‐Jene, L., Gersonde, R., Tiedemann, R., 2016. Pacific‐Atlantic Circumpolar Deep Water coupling during the last 500 ka. Paleoceanography 31, 639–650. https://doi.org/10.1002/2016PA002932

Veres, D., Bazin, L., Landais, A., Toyé Mahamadou Kele, H., Lemieux-Dudon, B., Parrenin, F., Martinerie, P., Blayo, E., Blunier, T., Capron, E., Chappellaz, J., Rasmussen, S.O., Severi, M., Svensson, A., Vinther, B., Wolff, E.W., 2013. The Antarctic ice core chronology (AICC2012): an optimized multi-parameter and multi-site dating approach for the last 120 thousand years. Clim. Past 9, 1733–1748. https://doi.org/10.5194/cp-9-1733-2013

Watson, A.J., Bakker, D.C.E., Ridgwell, A.J., Boyd, P.W., Law, C.S., 2000. Effect of iron supply on Southern Ocean CO_2 uptake and implications for glacial atmospheric CO_2. Nature 407, 730–733. https://doi.org/10.1038/35037561

Weber, M.E., Kuhn, G., Sprenk, D., Rolf, C., Ohlwein, C., Ricken, W., 2012. Dust transport from Patagonia to Antarctica – A new stratigraphic approach from the Scotia Sea and its implications for the last glacial cycle. Quaternary Science Reviews 36, 177–188. https://doi.org/10.1016/j.quascirev.2012.01.016

Weber, M.E., Clark, P.U., Kuhn, G., Timmermann, A., Sprenk, D., Gladstone, R., Zhang, X., Lohmann, G., Menviel, L., Chikamoto, M.O., Friedrich, T., Ohlwein, C., 2014. Millennial-scale variability in Antarctic ice-sheet discharge during the last deglaciation. Nature 510, 134–138. https://doi.org/10.1038/nature13397

Wessel P., Smith W.H.F., Scharroo R., Luis J.F., Wobbe F., 2013. Generic mapping tools: improved version released. EOS Trans AGU 94, 409–410.

Winckler, G., Lamy, F., Alvarez Zarikian, C.A., Arz, H.W., Basak, C., Brombacher, A., Esper, O.M., Farmer, J.R., Gottschalk, J., Herbert, L.C., Iwasaki, S., Lawson, V.J., Lembke-Jene, L., Lo, L., Malinverno, E., Michel, E., Middleton, J.L., Moretti, S., Moy, C.M., Ravelo, A.C., Riesselman, C.R., Saavedra-Pellitero, M., Seo, I., Singh, R.K., Smith, R.A., Souza, A.L., Stoner, J.S., Venancio, I.M., Wan, S., Zhao, X., and Foucher McColl, N., 2021. Expedition 383 summary. *In* Lamy, F., Winckler, G., Alvarez Zarikian, C.A., and the Expedition 383 Scientists, *Dynamics of the Pacific Antarctic Circumpolar Current*. Proceedings of the International Ocean Discovery Program, 383: College Station, TX. https://doi.org/10.14379/iodp.proc.383.101.2021

Xiao, W., Frederichs, T., Gersonde, R., Kuhn, G., Esper, O., Zhang, X., 2016. Constraining the dating of late Quaternary marine sediment records from the Scotia Sea (Southern Ocean). Quaternary Geochronology 31, 97–118. https://doi.org/10.1016/j.quageo.2015.11.003

Yamazaki, T., Ikehara, M., 2012. Origin of magnetic mineral concentration variation in the Southern Ocean. Paleoceanography 27, PA2206. https://doi.org/10.1029/2011PA002271

Yamazaki, T., Abdeldayem, A.L., Ikehara, K., 2003. Rock-magnetic changes with reduction diagenesis in Japan Sea sediments and preservation of geomagnetic secular variation in inclination during the last 30,000 years. Earth, Planets and Space 55, 327–340. https://doi.org/10.1186/BF03351766

Zielinski, U., Gersonde, R., 2002. Plio–Pleistocene diatom biostratigraphy from ODP Leg 177, Atlantic sector of the Southern Ocean. Marine Micropaleontology 45, 225–268. https://doi.org/10.1016/S0377-8398(02)00031-2